REVISTA ESPINHAÇO
ISSN 2317-0611
Revista Espinhaço, 2025, 15 (1)

The Paleoproterozoic diamond province of the southern Espinhaço range (Brazil): Primary and exogenous textures, mineral inclusions and genesis of diamonds

A Província diamantífera paleoproterozoica da Serra do Espinhaço Meridional (Brasil): Texturas primárias e exógenas, inclusões minerais e gênese dos seus diamantes

Anna Cecília Müller
UFVJM
https://orcid.org/0000-0002-1686-3893
annaceciliamuller@gmail.com

Eduardo Fontana
UFVJM
https://orcid.org/0000-0002-1963-7795
eduardo.fontana@ict.ufvjm.edu.br

Lucilia A. Ramos Oliveira
UFVJM
https://orcid.org/0000-0003-1295-6432
lucilia.oliveira@ict.ufvjm.edu.br

Pedro Angelo Almeida-Abreu
UFVJM
https://orcid.org/0000-0001-6273-4809
pangelo@ict.ufvjm.edu.br

José Maria Leal
UFVJM
https://orcid.org/0009-0008-8731-8623
jose.leal@ict.ufvjm.edu.br

Francisco Javier Rios
UFMG
https://orcid.org/0000-0001-5284-8714
javier@cdtn.br

Abstract

Although diamonds from the Diamantina district have been known and studied since the 18th century, their genesis, associated mantle processes and environmental context of the rise of kimberlites are still unknown. Furthermore, the nature and source area of these diamonds has been the subject of intense scientific debate for decades. Therefore, in order to add knowledge about the origin and history of diamonds from the Serra do Espinhaço diamond province, samples of diamonds from São João da Chapada and the Jequitinhonha River areas were studied in this work. The surface and infrared spectral characteristics of the studied crystals and the analysis of their mineral inclusions suggest that the sublithospheric (hence, cratonic) Jequitinhonha River diamonds crystallized in the peridotite mantle, since the presence of forsterite inclusion implies crystallization at temperatures of ~1170 ºC and pressure of ~65 kbar. Furthermore, the presence of flat-bottomed trigons

indicates that these diamonds reacted with H_2O-rich fluids during the final stages of the kimberlite emplacement. The abundant presence of ruts in São João da Chapada diamonds indicates crystallization conditions in highly oxidized volcaniclastic kimberlite, at temperatures of ~1040 ºC. The diamondiferous ruditic rocks of the Sopa-Brumadinho Formation were deposited around 1.7 Ga, therefore, the minimum age of the kimberlitic event. As cratonic diamonds reside for a prolonged period in the lithospheric mantle, the crystallization of diamonds from southern Espinhaço Mountain Range during the Neoarchean period (~3.0 Ga) is suggested.

Keywords: Diamond genesis; Kimberlite emplacement; Mantle processes; Espinhaço Diamond Province.

Resumo

Embora os diamantes do distrito de Diamantina sejam conhecidos e estudados desde o século XVIII, sua gênese, os processos mantélicos associados e o contexto ambiental da ascensão dos kimberlitos ainda são desconhecidos. Ademais, a natureza e a área fonte desses diamantes vem sendo, há décadas, objeto de intenso debate científico. Portanto, a fim de ampliar o conhecimento sobre a origem e a história dos diamantes da província diamantífera da Serra do Espinhaço, amostras de diamantes das áreas de São João da Chapada e do Rio Jequitinhonha foram estudadas neste trabalho. As feições de superfície e as características espectrais infravermelho dos cristais estudados e a análise de suas inclusões minerais sugerem que os diamantes sublitosféricos (portanto, cratônicos) do Rio Jequitinhonha cristalizaram no manto peridotítico, uma vez que a presença de inclusão de forsterita implica cristalização a temperaturas de ~1170 ºC e pressão de ~65 kbar. Além disso, a presença de trigons de base plana indica que esses diamantes reagiram com fluidos ricos em H_2O durante os estágios finais de intrusão do kimberlito. A presença abundante de sulcos nos diamantes de São João da Chapada indica condições de cristalização em kimberlito vulcanoclástico altamente oxidado, a temperaturas de aproximadamente 1040 ºC. As rochas rudíticas diamantíferas da Formação Sopa-Brumadinho foram depositadas por volta de 1,7 Ga, sendo, portanto, a idade mínima do evento kimberlítico. Como os diamantes cratônicos permanecem por um longo período no manto litosférico, sugere-se a cristalização dos diamantes da Serra do Espinhaço Meridional durante o período Neoarqueano (~3,0 Ga).

Palavras-chave: Gênese dos diamantes; Insertação de kimberlitos; Processos do manto; Província Diamantífera do Espinhaço.

1. Introduction

While Diamantina (Minas Gerais state, Brazil) was recognized as the world's leading diamond producer in the eighteenth century (Svisero, 2006), having yielded over four million carats between 1730 and 1830 (Renger, 2005), its green-coated diamonds have not been extensively studied with respect to their genesis. The source of these diamond deposits remains undiscovered, and their proximal or distal origin has been the subject of intense scientific debate for decades (Chaves and Svisero, 1993; Chaves et al., 1996; Chaves et al., 1998; Almeida-Abreu and Renger, 2001).

The diamond province from Southern Espinhaço range (SER) includes five diamondiferous districts along its mid-central area (Pflug, 1968; Schöll and Fogaça, 1979; Almeida-Abreu, 1993; Uhlein et al., 1998; Almeida-Abreu and Renger, 2002; Martins-Neto, 2009). The SER limits the southeast of the São Francisco Craton and encloses the oldest diamond province on the planet, with the age of diamond emplacement estimated between 1720 and 1680 Ma (ages of diamond host rocks, Dossin et al., 1993; Hagedorn, 2004; Bezerra-Neto, 2016).

At the northernmost diamond district of SER, in the São João da Chapada area, diamonds are stored in metaconglomerates and metabreccias of the Sopa Brumadinho formation (SBf). Furthermore, the alluvium of the drainage network in this region represents another source of diamond production, mainly from the Jequitinhonha River and its tributaries, providing diamonds mostly of gem quality.

Most diamond inclusion minerals originate in the sub-continental cratonic mantle lithosphere and only a small percentage of mineral inclusions originate beneath the lithosphere (~1%, Stachel and Harris, 2008). Inclusions in diamonds are classified as protogenetic (preceding diamond formation), syngenetic (co-crystallizing with diamond) or epigenetic (crystallizing after diamond formation).

Typically, a syngenetic origin for inclusions has been inferred if, regardless of their crystal system, the inclusions show a cuboidal-octahedral morphology that is imposed by their diamond hosts, which is most commonly the case (Walter et al., 2022). The fluid inclusions trapped in fibrous diamonds from the lithosphere report that the parental fluids exhibit a range in composition, including high- and low-Mg carbonatitic, chlorine-rich and silica-rich aqueous fluids (Walter et al., 2022). In a tight synthesis, it can be concluded that diamonds from the subcontinental lithosphere are formed under the metasomatism of carbonatitic or carbonated silicate melt (Babu et al., 2023). A somewhat similar conclusion was reached by Pintér et al. (2022) through experimental work, when they observed that the thick mantle lithosphere beneath cratons consists of strongly reduced rocks that have reacted with oxidized melts. The low-silica, incipient melts are rich in CO_2 and H_2O and react with surrounding rocks forming an enriched zone at the base of the lithosphere, which is the source region for many diamonds. Also referred to as an alternative mechanism to subducted or delaminated crust, or underplating by voluminous silicate magmas for the formation of pyroxenitic garnet and clinopyroxene inclusions in some lithospheric diamonds.

The surface characteristics of diamonds preserve records of processes that left marks on the crystals during their formation and rise to the surface of the Earth's crust. These characteristics imprinted on the diamond convey relevant information, such as (i) reabsorption induced by kimberlitic magma in the mantle environment; (ii) the physicochemical conditions during the rise of kimberlitic magma; and (iii) abrasion marks during transport on the earth's surface (Shirey et al., 2013).

Particularities about the mantle environment where diamonds are formed can be investigated through impurities left in their crystallographic structure, especially nitrogen and mineral inclusions, which can be detected by infrared (IR) analysis (Howell et al., 2013). Syngenetic mineral inclusions can be regarded as a virtual window into the Earth's mantle at the time of diamond crystallization. On the other hand, protogenetic and epigenetic inclusions materialize the environmental conditions

before and after diamond formation, respectively (Nestola et al., 2017). In this way, relevant data about the chemical composition, redox and stable phases of the mantle environment and geodynamic processes pertinent to the emplacement of kimberlites can be retrieved (Alvaro et al., 2022).

Diamonds from the São João da Chapada district of SER carry information about the physicochemical characteristics of the ancient Earth's mantle. Therefore, this work addresses data on the spectral properties of the studied diamonds, including the physical characterization of the crystals and their mineral inclusions. With the integration of analytical results, we seek to achieve unprecedented knowledge about the genesis and rise of green-capped diamonds from the São João da Chapada district, as well as information regarding processes related to transport on the Earth's surface. The studies included samples of diamonds obtained from "primary" rocks of the SBf (quartzite metabreccias with pelitic matrix) and diamonds from the Jequitinhonha River (JR). The analyses were performed using magnifying glass and a binocular microscope, in addition to Scanning Electron Microscopy (SEM) equipped with energy dispersive X-ray spectroscopy (EDS) and backscattered electron detectors (BSE), and also Fourier Transform Infrared Spectroscopy (FTIR).

2. Geological setting

The São Francisco Paleocontinent configuration results from Archean blocks amalgamation and records the consolidation of Gondwana in southeastern Brazil. The São Francisco Paleocontinent constitutes one of the five chronic units of the South American Platform (Almeida et al., 1981).

The Espinhaço Range has been the focus of several works (with emphasis on its southern segment) since the 18th century following the important discovery of diamond and gold deposits.

The SER is a Mesoproterozoic orogenic belt that limits the southeast of the São Francisco Craton (Herrgesell and Pflug, 1986; Almeida-Abreu and Renger, 2002), which extends for about 300 km from Belo Horizonte to the north of Diamantina city (Fig. 1). The Espinhaço Supergroup is composed of metarenites/quartzites, phyllites, metaconglomerates, iron formations and metavolcanic rocks metamorphosed into greenschist facies. The Espinhaço System integrates lithological units that make up the main building of SER and thrust belts that border the east of the mountain range (Herrgesell and Pflug, 1986; Almeida-Abreu and Renger, 2007; Rolim et al., 2016). Guinda and Conselheiro Mata groups (Dossin et al., 1984; Knauer, 1990) represent the Espinhaço Supergroup in the SER itself (Fig. 1 and 2). The Guinda Group, a succession deposited during the rift phase of the Espinhaço basin (Dussin and Dussin, 1995; Martins-Neto, 1998), or a remnant of a large coastal plain adjacent to the Espinhaço marine basin (Almeida-Abreu and Renger, 2007), encloses the São João da Chapada, Sopa Bumadinho and Galho do Miguel formations (Pflug, 1968) (Fig. 2). The Conselheiro Mata Group brings together the Santa Rita, Córrego dos Borges, Córrego Bandeira, Córrego Pereira, and Rio

Pardo Grande formations (Pflug, 1968), interpreted as a consequence of the thermal contraction of the basin (Martins-Neto, 2009) or as deposited in a foredeep basin related to the Espinhaço orogeny (Almeida-Abreu and Renger, 2007). The propagation of thrust sheets from the east over the ancient coastal plain during the Espinhaço orogeny originated a tectonic stacking of more than 8 km of rocks (Amaral-Santos et al., 2022), imposing regional metamorphism with temperatures of 450 ºC and pressures of 4-5 Kb (Schöll and Fogaça, 1981).

Figure 1. Simplified geological map of the SER

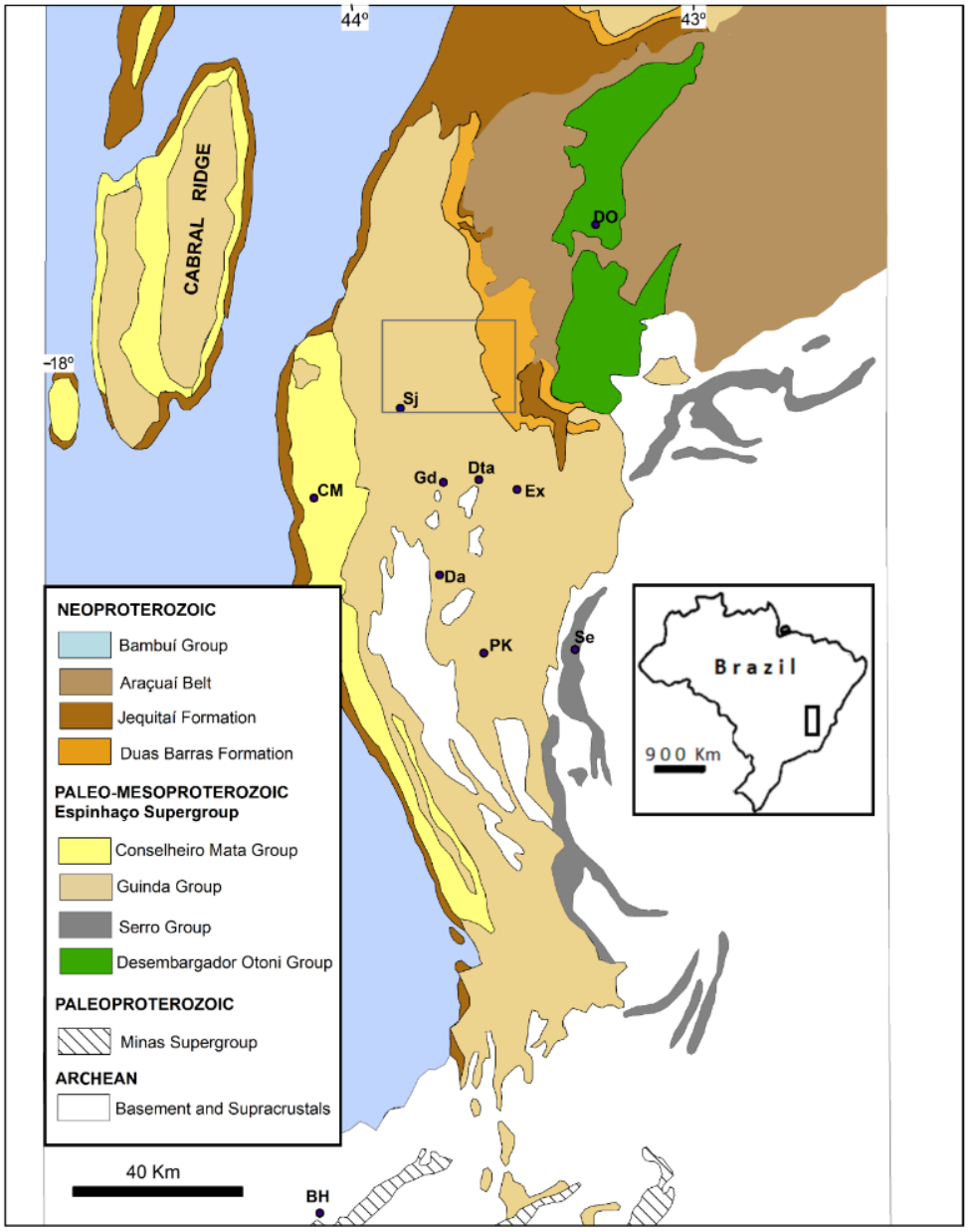

The rectangle delimits the area of Fig. 2. Towns and villages indicated on the map: CM – Conselheiro Mata; Da – Datas; DO – Desembargador Otoni; Dta – Diamantina; Ex – Extração; Gd – Guinda; PK – Presidente Kubitschek; Se – Serro; SJ – São João da Chapada.

This work presents the results of studies of the spectral properties of SER diamonds, including the characterization of their surface features and mineral inclusions of crystals arising from metabreccias of the SBf (Fig. 2) (Córrego Novo mine, district of São João da Chapada) and alluvium of the Jequitinhonha River (Fig. 2) (Areinha mine). Photographs of the analyzed diamonds are shown in this article, as well as photographs of metabreccia with the precise location where the studied diamonds were obtained (Supplemental Material Figures S1 to S5).

Figure 2. Geological map of the north-central area of the SER (Adapted from Projeto Espinhaço, 1997)

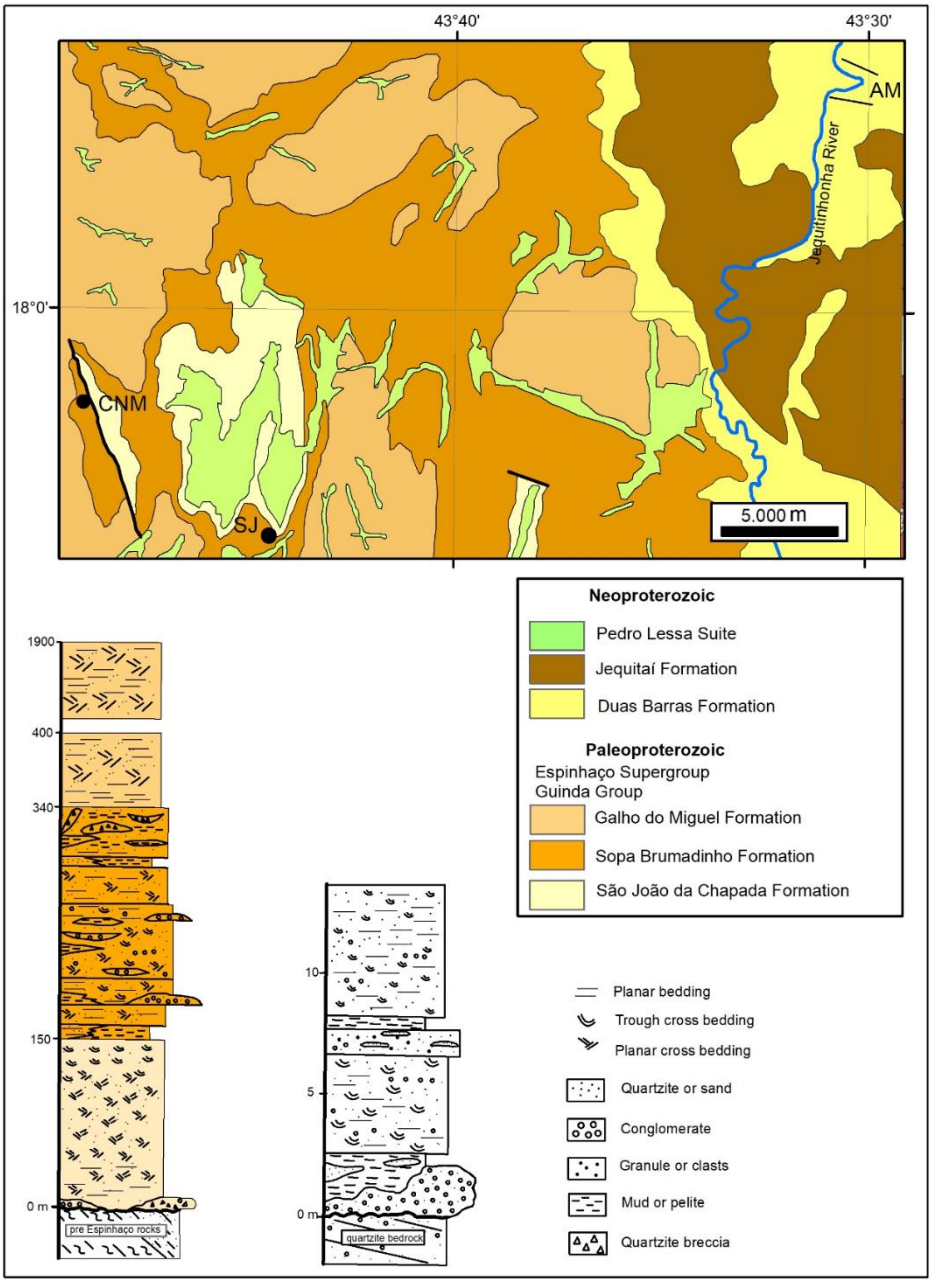

CNM indicates SJ diamond sampling area (Córrego Novo Mine) and AM indicates the JR diamond sampling area (Areinha Mine). The stratigraphic column on the left shows the lithologies of the three lower formations of the Espinhaço

Supergroup that outcrop in the area of the geological map. The conglomerates (from an alluvial fan environment) and breccias (vent-breccias) of the Sopa Brumadinho Formation are diamond-bearing. The Galho do Miguel Formation is composed of a thick succession of eolian sandstones. The stratigraphic column on the right shows the alluvial succession of the middle course of the Jequitinhonha river containing diamond-bearing gravels deposited on the bedrock.

2.1. Diamonds in the Geological Context of the Southern Espinhaço Range

The relationship of kimberlite magmatism to the supercontinent cycle has been well documented (e.g., Gernon et al., 2023), especially during the fragmentation of amalgamated masses. The diamond deposits in the east of the São Francisco Craton could therefore be related to the fragmentation of the Columbia/Nuna supercontinent and, according to geochronological results, occurred between 1,750 Ma (Hagedorn, 2004) and 1.7 Ga (Dossin et al., 1993), which, from the perspective of the experimental results of Gernon et al. (2023), kimberlitic magmatism was associated with the rifting process about 30 million years after continental breakup. Nonetheless, the precise age of the kimberlite event responsible for the mineralization of the SER diamond province is not yet available, however, within the SER, diamonds are not found in any older or younger rocks relative to the ruditic rocks of the SBf. Information about when the formation and crystallization of these diamonds occurred in the mantle environment is also lacking. As highlighted by Smit et al. (2022), diamonds from São Francisco craton still need diamond-dating studies. Since diamonds as old as 3.3 - 3.5 Ga are known from the Slave craton (Timmerman et al., 2022), it cannot be ruled out that the SER province diamonds were formed in the lithospheric mantle during Archean or Paleoproterozoic times.

Despite the restricted quantities and small dimensions of the stones, the presence of diamonds in Archean deposits is also well documented, therefore indicating kimberlitic magmatic events mainly in the Late Archean (~2.6 billion years), during the peak of the first cratonic formation on Earth (Lefebvre et al., 2005).

Even older diamonds, ca. 3.0 Ga, records a kimberlitic magmatic event at the beginning of the Archean period (Smart et al., 2016), while detrital microdiamonds recovered from the basal conglomerate that rests in the Slave Craton show a combination of high values of $\delta^{13}C$ and $\delta^{15}N$, demonstrating the presence of crustal marine carbonate taken to depths >170 km, possibly through subduction processes (Timmerman et al., 2022), while Pintér et al. (2022) pointed out that the thick mantle lithosphere beneath the cratons — the ancient cores of the continents — has cold, stable roots reaching ~250 km depth, which consists of strongly reduced rocks that have reacted with oxidized incipient melts with low-silica, and rich in CO_2 and H_2O. The reaction of the melts with the surrounding rocks forms an enriched zone at the base of the lithosphere, which is the source region for many diamonds, therefore, diamonds reside in the lithospheric mantle beneath cratons, and the intersection of peridotite derived conductive geotherms with the diamond stability field, led to the

suggestion that diamonds have formed through nearly all of Earth's history in distinct episodes that can often be linked to larger-scale tectonic processes (Smit et al., 2022).

The assumption that diamonds are formed primarily by the supply of organic carbon from the crust through the subduction process allows us to speculate about the increase in the quantity and size of diamonds over the course of Earth's evolution. Therefore, it does not seem accidental that the first robust deposits of diamonds with crystals measuring centimeters to decimeters occur from the end of the Paleoproterozoic (SER province) and especially the Mesoproterozoic epoch (Premier kimberlite and lamproites from Ellendale and Argyle) and with notable growth in quantity and volume of diamond deposits during the Phanerozoic. Smit et al. (2022) consider the 1153 Ma Premier kimberlite to be the first to contain sublithospheric diamonds and furthermore, as their CLIPPIR diamonds carry metallic inclusions of heavy Fe isotopic compositions linked to serpentinite, relating them to modern-style plate subduction. Therefore, they admit a process of subduction of modern-style plates since at least the Mesoproterozoic.

The diamond province of SER in Minas Gerais state was considered by Benitez (2009) as four larger diamond districts: Diamantina, Grão Mogol, Jequitaí and Itacambira. However, the Diamantina region itself, i. e., the SER, comprises five diamond-bearing districts, named as follows: São João da Chapada-Campo Sampaio, Sopa-Guinda, Extração, Datas and Presidente Kubitschek (Almeida-Abreu and Renger, 2001). The diamond-bearing Precambrian rocks in these districts are metaconglomerates and metabreccias of the SBf (Fig. 2), although the colluvium and alluvium of the drainage system had high concentrations of diamonds. In the district of São João da Chapada-Campo Sampaio the Precambrian diamondiferous rocks are restricted to the quartzite metabreccias, that occur in the uppermost part of the SBf. The occurrence of diamonds with sub-economic content is noteworthy in some syn-sedimentary volcanic rocks, such as hematite phyllites and similar rocks (Correns, 1932; Almeida-Abreu and Renger, 2001; Bezerra-Neto, 2016).

In the diamond districts, several mines remained in operation from the mid-19th century until the early 1980s. The Quaternary erosion of Precambrian diamondiferous ruditic rocks promoted the mineralization of colluvial and alluvial deposits, especially of the Jequitinhonha River and its tributaries that originate in the mid-central part of the SER. The SBf metabreccias occur in different parts of the SER, however the largest deposits of economic interest are restricted to the diamondiferous deposits of São João da Chapada and Sopa-Guinda (Almeida-Abreu and Renger, 2001). SBf metabreccias were classified as debris flow deposits by Chaves and Svisero (1993), however diamond mineralization in these rocks is pervasive, with the breccia matrix showing an invariable pelitic composition and its clasts are invariably very angular (Supplemental Material, Figure S3), that is, of autochthonous or proximal origin. Therefore, the assumption that these breccias

are cohesive debris flows refers to the proximal reworking of primary diamond-bearing rocks. Furthermore, in some locations small intrusive pipes are preserved as dikes in the SBf metasandstones and phyllites, suggesting their origin as vent breccias resulting from phreatomagmatic eruptions (Almeida-Abreu, 1996; Almeida-Abreu and Renger, 2001; Miranda et al., 2019). The bodies of these metabreccia, despite variable thickness and lateral distribution, present a predominantly irregular geometry, sometimes resembling the configuration of a champagne glass, surrounded by the host rocks, that is, phyllites and meta-sandstones of the SBf.

3. Materials and methods

Diamonds from metabreccias of the Córrego Novo mine (São João da Chapada district - SJ1 to SJ13) and from alluvial deposits of the Jequitinhonha River (Areinha mine - JR1 to JR11) were analyzed with the aid of a digital magnifying glass and a binocular stereoscopic microscope in the Mineralogy Laboratory of the Center for Geoscience Studies (CeGeo) of the Federal University of Vales do Jequitinhonha and Mucuri (UFVJM). The morphology of diamonds was described, including coat, stains, habit, and surface characteristics. These diamonds were also subjected to ultraviolet light to enhance the study of their mineralogy by measuring fluorescence, which can indicate the presence of diamond impurities (nitrogen). Ten crystals were separated and polished with a steel scaife. After polishing, the diamond platelets were then cleaned with an ultrasonic bath for subsequent petrographic study using a polarized light microscope.

Additional analyses were conducted using a Scanning Electron Microscope (SEM) with energy dispersive spectroscopy (EDS), backscattered detectors (BSE) and secondary electrons (SE) at the Nuclear Technology Development Center (CDTN) and at UFVJM, using a VP SIGMA and a HITACHITM 3000, respectively.

Fourier transform infrared spectroscopy (FTIR) was performed at the Federal University of Goiás (UFG) using a Bruker Vertex 70 spectrometer. The spectra were acquired in the spectral band of 4000 - 400 cm^{-1}, with a resolution of 4 [cm^{-1}]. The FTIR spectra was subjected to baseline correction and normalization using the Quiddit software (Speich and Kohn 2020).

Spectra deconvolution was also performed using Quiddit to obtain information on the state of nitrogen aggregation, the temperature model, and platelet peak position. Absorption coefficients for A and B-centers were extracted according to Boyd et al. (1994, 1995). Model temperatures were determined based on both nitrogen aggregation and platelet degradation. The former was calculated according to Taylor et al. (1990, 1996), and the latter was calculated according to Speich et al. (2018). Data analysis and database searches on the RRuff Mineral (Lafuente et al., 2015) were conducted using the Spectragryph software developed by Friedrich Menges (http://spectroscopy.ninja).

4. Results

4.1. Morphology and Surface Textures of the Analyzed Diamonds

Diamonds from the São João da Chapada district are easily identified by their distinctive green coating (Fig. 3 and Supplemental Material Figure S1), an evenly spread translucent green color limited to the surface of the diamond. In the samples examined, this green coat often coexists with green spots and, additionally, some SJ diamonds in their natural form exhibit a fibrous structure or a fibrous coat (Fig. 3). These fibers on the diamond's coat are observable without magnification and, like most fibrous diamonds, are recognizable by their characteristic dull appearance (Fig. 3a, b). Mineral inclusions in SJ12 diamond fibers are visible, with one of these minerals having an orange hue, while the other has a black color with a metallic luster (Fig. 3a, b). On the other hand, the irregularly shaped diamond SJ1 displays, in the polished section, a thick fibrous layer (Fig. 3c), whereas in SJ3 diamond the microscopic fibers fit to the octahedral habit of the crystal (Fig. 3d).

The set of diamonds from São João da Chapada district (SJ) exhibit sizes ranging from 2.5 mm to 4 mm and have a rounded octahedral habit. The most common surface features are steps, ruts (Fig. 4a, b, c), negative flat-bottomed trigons (Fig. 4d) and frost, and many fractures with different directions are also common. Most samples have submillimeter-sized green spots on the surface, and in some samples the spots are clustered together, forming large stains (Fig. 4a, b, c, d). Similar features are found in samples SJ4, SJ7, SJ8 and SJ9, with sample SJ7 additionally showing frost, while samples SJ10, SJ11, SJ12 do not show negative trigons and twinning. Sample SJ13 (Fig. 4d), on the other hand, shows negative trigons, frost, and stepping. All SJ samples present ruts, except SJ12 and SJ13.

Figure 3. Images of fiber-coated diamonds from the SJ set.

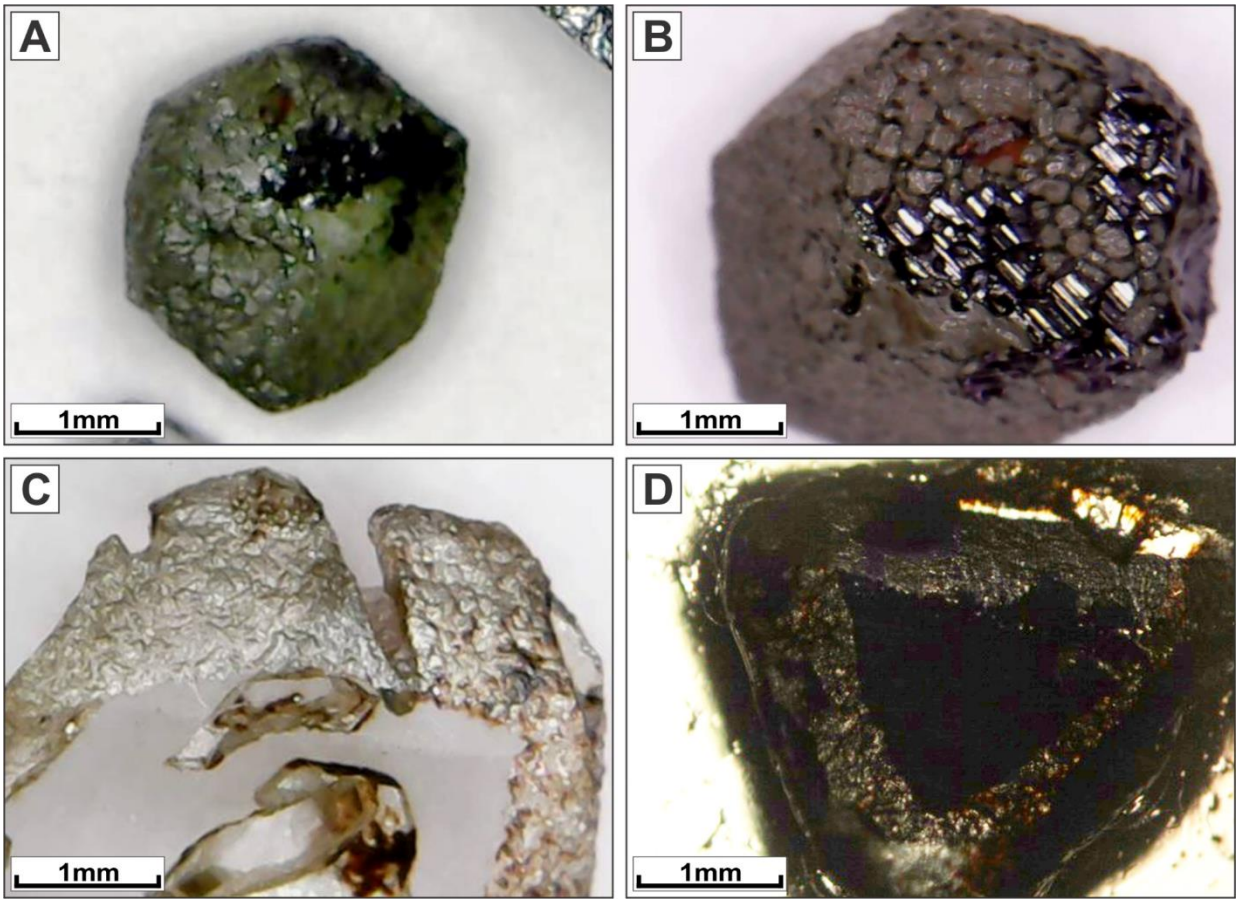

A) Diamond SJ12 with its green layer and fibrous texture; B) Detail of the diamond shown in (A), where mineral inclusions are lodged in its fibers (in orange and black colors; C) Polished section of diamond SJ1, showing a thick fibrous layer, two grooves on the top and two translucent mineral inclusions in the center; D) Polished section of octahedral diamond SJ3, which exhibits a thick fibrous layer.

Figure 4. Images of SJ and RJ diamonds displaying their more representative surface characteristics

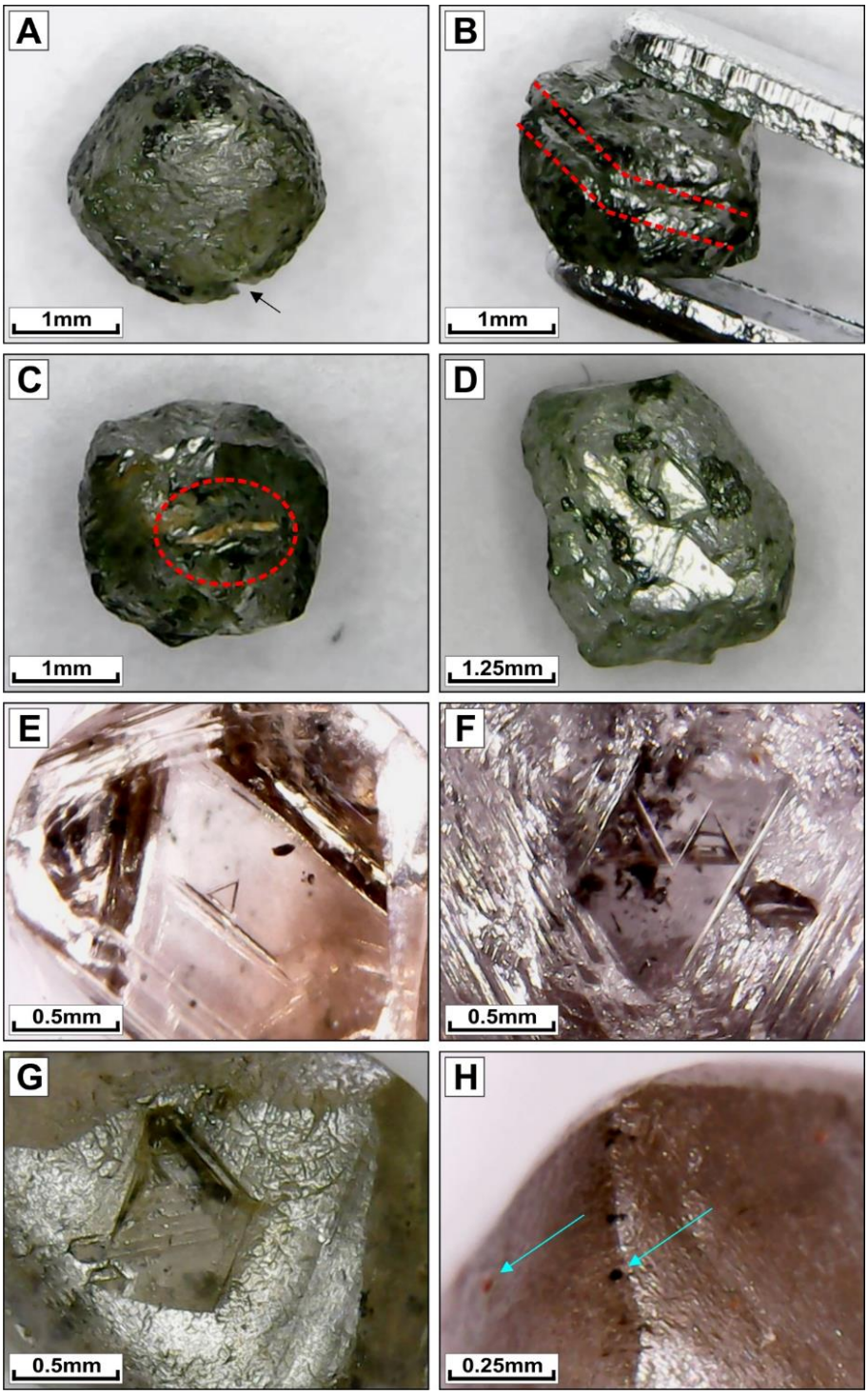

A) SJ5 diamond with green coating showing a rut (arrow), as well as several green spots distributed under its rough surface; B) view from another angle of the SJ5 diamond with visualization of a quartz-filled rut (between the dashed red lines); C) Irregular-shaped green coated SJ7 diamond presenting green spots and a rut filled with clay minerals (inside the circle); D) Green coated SJ13 diamond revealing irregular habit, large green spots and negative trigons; E) Octahedral JR2 diamond exhibiting a positive trigon and stepping into its center and corners; F) JR3 Diamond exhibiting trigons in the center, hillocks distributed on the face´s edges, and a large scratch mark on the right; G) Green coated JR4 diamond with terraced triangle, green spots, and numerous percussion marks across the surface; H) Edge of JR4 diamond showing green spots and abrasion marks, and a single brown spot (right arrow).

The Jequitinhonha River (JR) diamonds show dimensions between 4.0 mm and 8.5 mm, with half of this set being green-coated diamonds and, furthermore, most of these crystals have an octahedral habit and a lower degree of roundness. Their main surface features are stepping (Fig. 4e), trigons (Fig. 4e, f, g), frost and percussion marks (Fig. 4g), but fractures and scratch marks (Fig. 4f) are also present in some of these crystals. The JR4 sample displays non-centered terraced trigons in a truncated manner (Fig. 4g) that are present in smaller numbers and larger sizes compared to the other trigons seen in samples of this set. This sample shows elongated hillocks on the dodecahedral crystal face, oriented towards the edges of the relict octahedral crystal face (Fig. 4g). Some of these diamonds are green-coated and possess green spots on their surface, but only the sample JR4 has green and brown spots in the same crystal (Fig. 4h). The relevant distinction between SJ and RJ diamonds lies in the exogenous transport characteristics, given that RJ diamonds almost invariably show percussion and abrasion marks (Fig. 4g, h and Fig. 5). Samples JR3 and JR4 exhibit notable brown spots, while diamond JR3 has a smooth surface.

Surface features and morphological characteristics found in the studied diamonds were summarized and schematized in Fig 5. The diagram shows the simplified representation of diamond sets of São João da Chapada and the Jequitinhonha River, highlighting the most recurring features and textures recognized, where it is possible to observe that the SJ diamonds are more fractured and rutted, while the JR ones have percussion marks as an exclusive characteristic. Tables in figures S6 and S7 of the Supplemental Material list features and textures found in diamonds from the SJ and JR sets, respectively.

Figure 5. Graphical representation of the most common surface textures and imperfections observed in SJ and JR diamonds, which shows similarities with texture representations presented by Tappert and Tappert (2011) and Fedortchouk (2019).

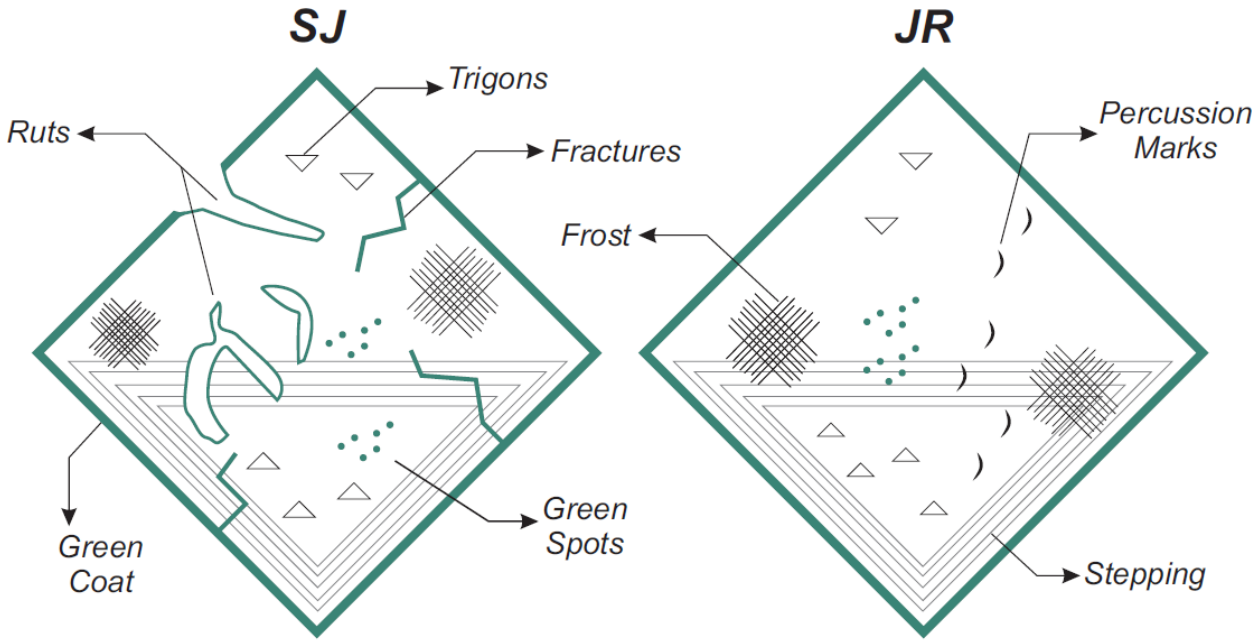

Explanation of terms: *Rut* - channel-shaped cavity without preferential crystallographic orientation; *Trigons* - triangular cavities; *Stepping* - diamond face with multiple successive layers; *Frost* - face like the surface of an ice cube; *Percussion Marks* - millimetric arc-shaped scratches; *Green Spots* - isolated or clustered sub millimetric stains; *Green Coat* - green-colored diamond surface; *Fractures* - linear cracks on the diamond surface with no preferred crystallographic direction.

5. Scanning electron microscopy

5.1. Morphology and Surface Textures

SEM images of the SJ and JR diamonds provided a broad, panoramic view of their surface features. Microchannels of different widths filled with clayey granular material were observed on one side of the SJ2 sample, often defining a polygonal shape (Fig. 6a), and between these microchannels a thin surface feature can be observed, forming overlapping steps with angular edges (Fig. 6a). In the high-detail image of the JR10 diamond, ruts or etch-channels can be seen on the edge of this sample, and such ruts define rounded to angular shapes and are filled with material of different composition. In Fig. 6c and d (sample JR3) two distinct surface texture features are observed, that is, the occurrence of negative terraced trigons is seen in the right part of the image, while wavy-like and drop-like hillocks are observed close to the surface of this crystal (Fig. 6c, d). In the other samples, this texture when present has more rounded shapes with larger droplet shapes.

Figure 6. SEM images showing surface features of SJ and JR diamonds

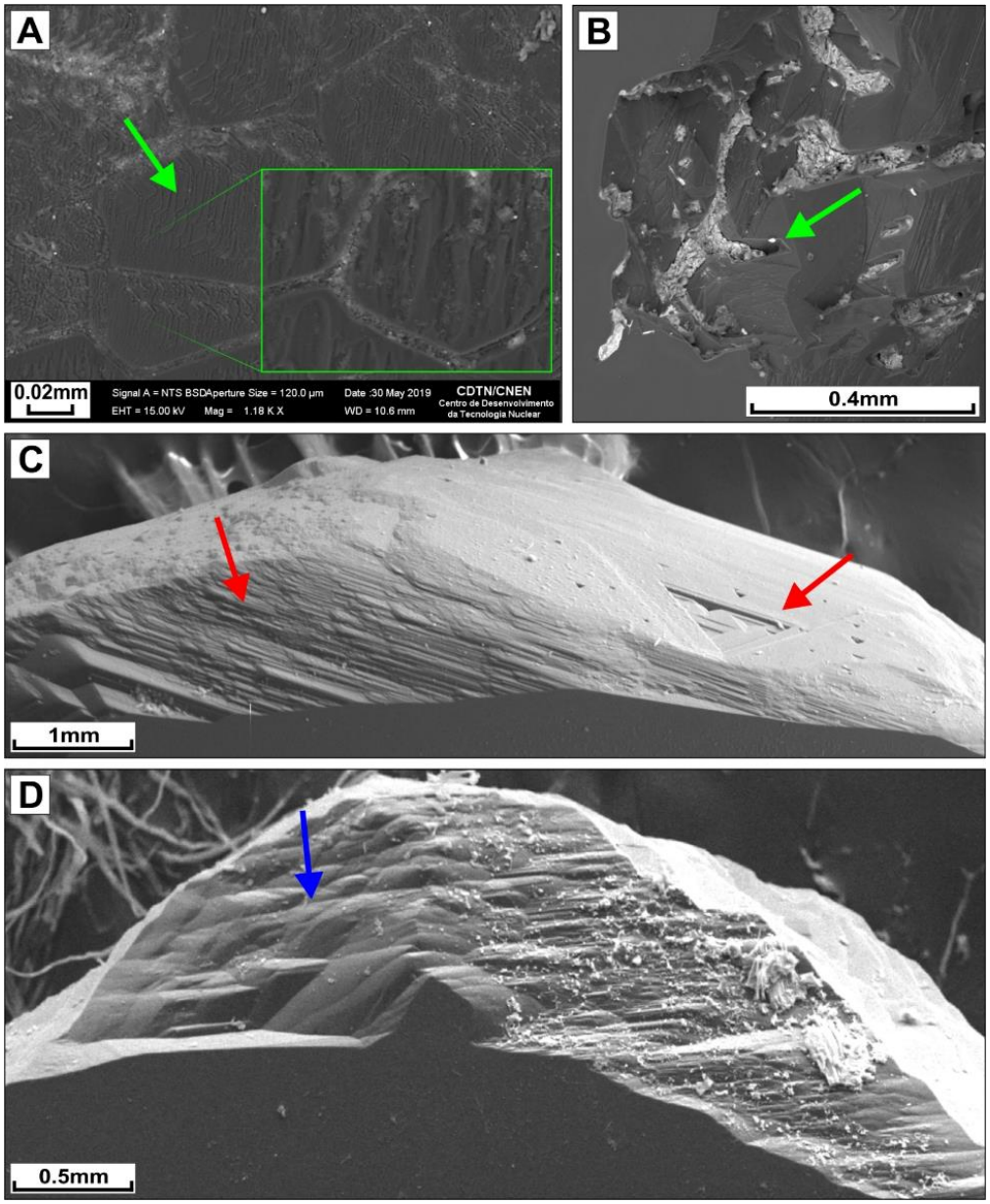

a) Image of polygonal-shaped dissolution microchannels on the surface of SJ2 diamond filled with a material of different composition. The fine surface texture displays steps in overlapping beds and angular edges (arrow); b) Edge of the JR10 diamond where ruts forming angular to rounded shapes are observed filled with material of different composition; c) Surface of JR3 diamond showing terraced trigons (right arrow) and numerous hillocks in parallel arrangement (left arrow); d) detail of the hillocks (arrow) of the image shown in (c).

5.2. Ruts

High-resolution SEM/EDS images reveal deep etch-channels called ruts, which are present in almost all SJ diamonds. These channels are between 100 and 300 µm wide, with depths that can reach up to 700 µm. Seen on the surface of diamonds, the ruts have a linear or slightly arched shape and are up to 1000 µm long (Fig. 7a). Scanning electron microscope (SEM) images revealed that most of the ruts are filled with quartz, as seen in Fig. 7b, c, and d (additional data is provided in Supplemental

Material Figure S8). Furthermore, as the polishing planes intersect the ruts at different angles, their morphology and interactions with the diamond edges become exposed. The images in Figures 7c and d show two distinct ruts from a polished section of the SJ1 diamond, both filled with quartz. The EDS analysis (spots 9 and 7 of Fig. 7c, d) indicated the same composition of Si and O. On the other hand, the fibrous coating of SJ1 diamond has a different chemical composition, given the presence of Na, Mg, Al and O (Fig. 7e), and in this same image (Fig. 7e) the bipyramidal prismatic mineral shows a composition (obtained by SEM) of Ca, Fe, Na, Mg, Al, Si and O. The image also shows that this mineral was sectioned by a surface feature, i. e., a rut (additional SEM images can be seen in Supplemental Material Figure S9).

Figure 7. SEM images of SJ diamond ruts.

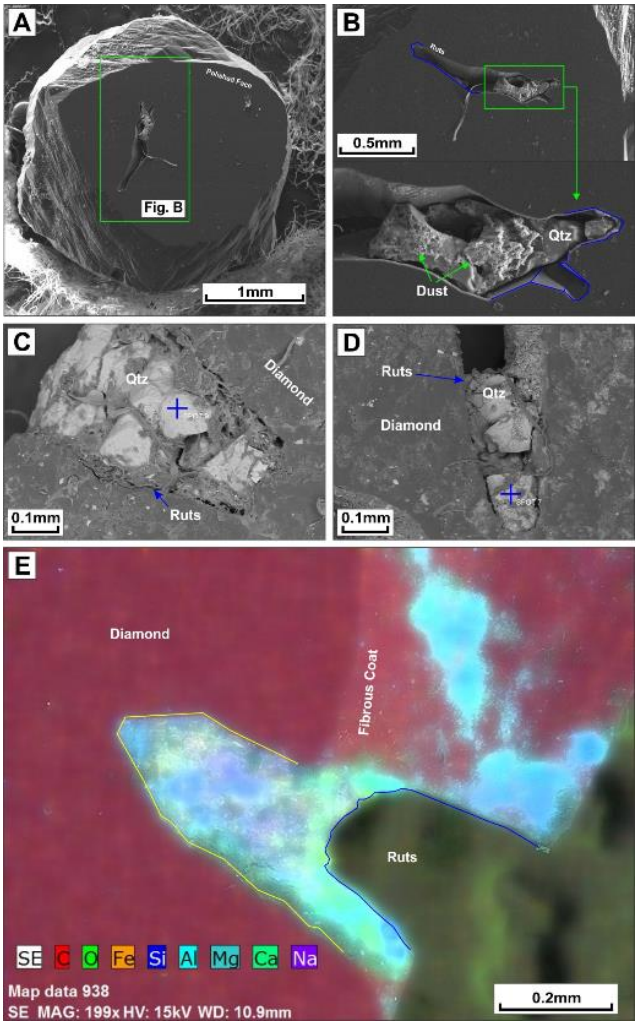

A) Plan view of polished section of SJ7 diamond showing a rut in the central part of the section; B) Detail of the rut shown in (A), where it can be seen that part of the channel is filled with quartz; C) Polished section of SJ1 diamond showing rut on its edge filled with mineral with quartz composition (Si and O); D) Another rut also located on the edge of SJ1diamond and also filled with quartz; E) Chemical element map (obtained by EDS) of the polished section of another edge of the SJ1 diamond, where a rut is filled, in part, by a prismatic mineral. The areas of the section dominated by the fibrous coat present chemical elements similar to those of the prismatic mineral. The legend at the bottom left of the image indicates which colors are used to represent the identified chemical elements.

5.3. São João da Chapada and Jequitinhonha River Diamonds FTIR Analysis

FTIR analysis was performed on seven diamonds from the SJ and JR sets. The analyses revealed that both sets include diamonds of type IaA (SJ1, SJ2, SJ3, JR5) and diamonds of mixed type IaAB (SJ7, JR2, JR10). The JR2 diamond spectrum is plotted in Fig. 8, where the characteristic peaks of type A (1282 cm-1) and type B (1175 cm-1) nitrogen-containing defects are highlighted. Comparative data revealed a similarity of 68.38% between a part of the JR2 diamond spectrum and a forsterite spectrum (Fig. 8). Spectral graphs for the other SJ and JR diamonds mentioned can be found in Supplemental Material Figure S10. The SJ1 diamond had a nitrogen concentration of 274 ppm, while three diamonds from the Jequitinhonha River had a nitrogen concentration between 120 ppm and 220 ppm. Based on these nitrogen contents, the model temperatures determined were 1177 ºC for one SJ diamond and 1164 ºC to 1177 ºC for the three RJ diamonds, assuming a mantle residence time of 3 Ga. The assumed residence period was based on Archean ages reported for cratonic harzburgitic and eclogitic diamonds (McKenna et al., 2004).

Figure 8. Diamond JR2 spectrum plot highlighting the characteristic A-type (1282 cm-1) and B-type (1175 cm^{-1}) peaks related to nitrogen-containing defects.

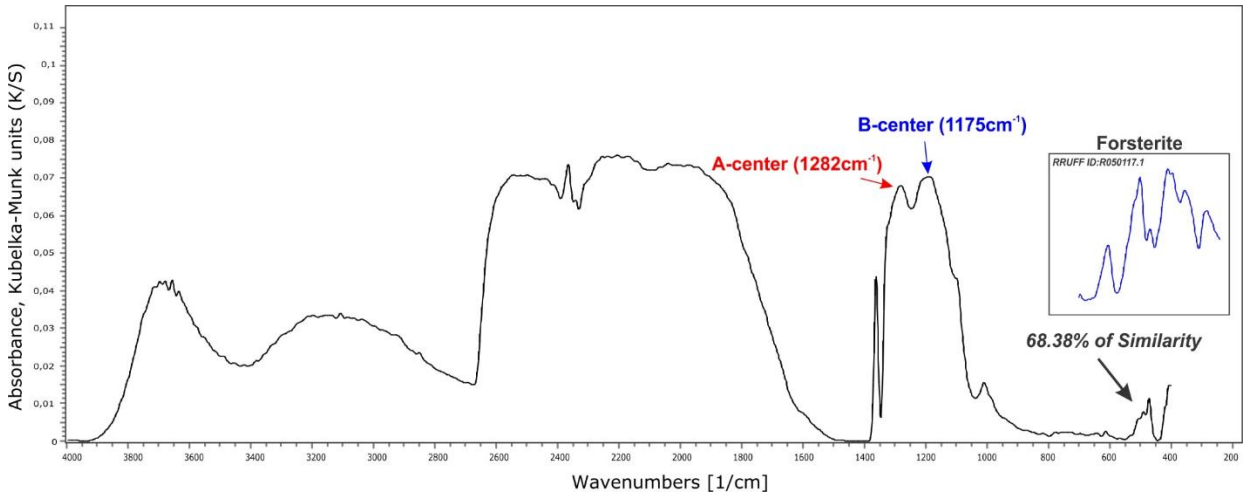

The upper right rectangle shows an amplified spectrum of forsterite (blue line) that overlaps the JR2 spectrum range between wavelengths of 700 and 400 cm^{-1}.

5.4. Mineral Inclusions

A conventional transmitted light optical microscopy analysis (natural and polarized) on JR diamonds (Fig. 9) showed that these samples contain opaque and translucent mineral inclusions with distinct characteristics such as size, shape, and crystal orientation. In samples JR10 and JR3, dark and opaque inclusions are clustered near the edges of the crystal, appearing rounded and elongated (sometimes placoid), with well-defined boundaries, while smaller inclusions exhibit a teardrop shape

and diffuse contacts (Fig. 9a, b). In the polished section of the JR10 sample the distribution of mineral inclusions appears to form an angle similar to that of the diamond face. In this same polished section, the presence of material with an orange hue was also noted, presenting a rusty appearance. In samples JR7 and JR5, the opaque inclusions show remarkable variation in size, distribution, and shape (Fig. 9c, d), which may also appear as clusters in the central zone of the host crystal and show a placoid and rounded shape following different directions of the diamond crystallographic joints. An orange-hued mineral inclusion with a rusty appearance can be observed (Fig. 9c, d), while opaque inclusions following the diamond's crystal structure and with sinuous terminations appear in Fig. 9e, f and g.

Figure 9. Photomicrographs of JR diamonds highlighting their mineral inclusions

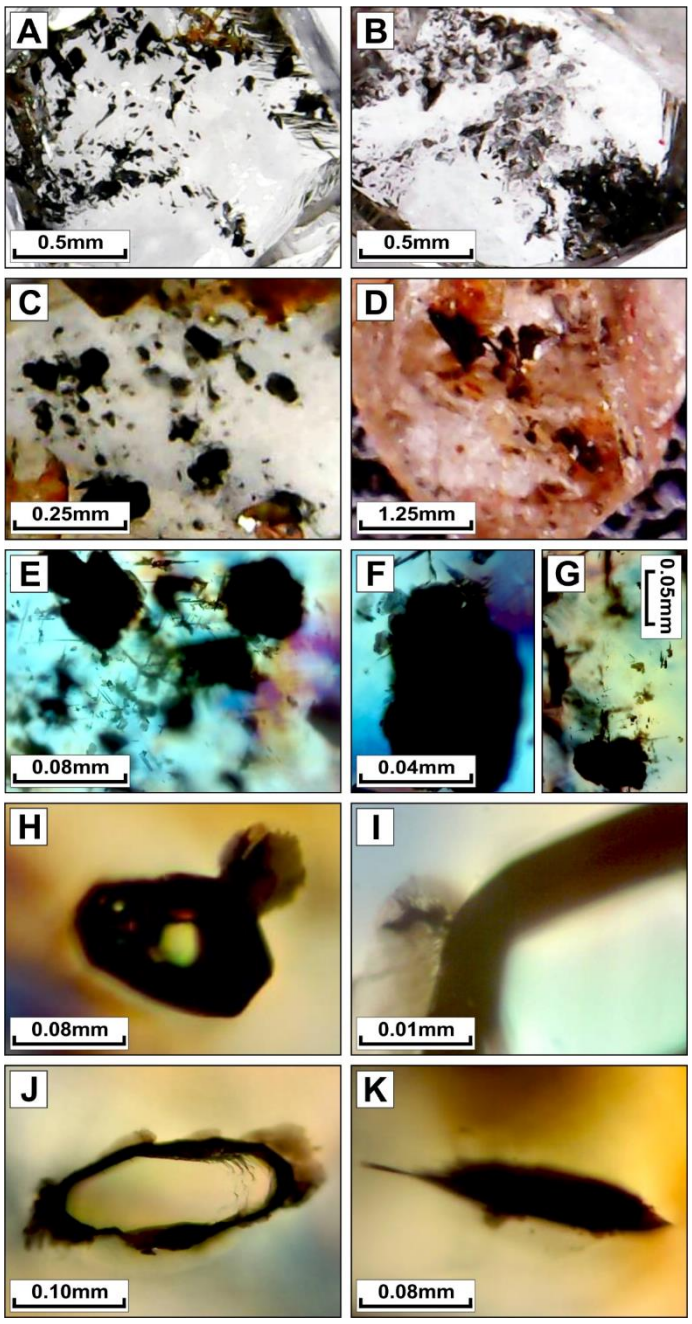

A) Polished section of sample JR10 showing opaque mineral inclusions with irregular placoid habit, which are arranged mainly at an angle similar to that of the diamond face. In the upper part of the image, an orange spot looks somewhat rusty; B) Polished section of JR3 diamond showing opaque mineral inclusions clustered at the edges of the crystal; C) Polished section of the JR7 diamond showing opaque dark mineral inclusions with a rounded shape and placoid habit. Orange-toned stains can be seen in the upper and lower right parts of the image; D) Polished section of the JR5 diamond showing dark-colored inclusions with a rounded placoid shape and highlighting dark orange stains in the peripheral parts of the crystal; E) Polished section of JR7 sample viewed under polarized light. It displays larger, rounded, dark mineral inclusions with a placoid habit, while the smaller mineral inclusions exhibit an acicular habit distributed according to the crystallographic joints of the diamond; F) Image under polarized light of one of the largest inclusions of the JR7 sample showing an ellipsoidal shape and irregular contour; G) Detail image under polarized light of the two types of inclusions from the JR7 sample mentioned above. Note the acicular inclusions protruding from the larger opaque inclusions; H) Transmitted light image of the JR2 sample, highlighting two euhedral translucent inclusions that appear twinned and surrounded by a dark halo. Note that dendritic minerals are associated with the inclusions and fractures that surround them; I) Magnification of the image of the JR2 sample showing a dark dendritic mineral in contact with the translucent mineral inclusion; J) Detail of a face of JR2 diamond showing an elongated translucent mineral inclusion and apparent growth in concentric beds. Dark halo and black dendritic minerals associate with fractures around the mineral layer; K) In another area of the JR2 diamond face, an isolated dark mineral is observed, with an elongated placoid shape.

On the other hand, smaller mineral inclusions have an acicular habit that follows the internal limits of the crystal joints and some of these mineral inclusions, under polarized light, exhibit a rounded shape and brownish tone, suggesting that they are a transitional mineral phase or a distinct opaque mineral.

In sample JR2, a translucent mineral inclusion was observed in natural transmitted and polarized light and two of these inclusions appear to be twinned and have a dark halo around them (Figure 9h) and, in addition, a dark reddish-brown mineral with an apparent dendritic habit occurs associated with the translucent mineral. This dark mineral always occurs at the limits of crystalline contact between the translucent mineral inclusion and the host diamond and is always surrounded by fractures that appear to be filled by the same dark mineral inclusion (Fig. 9h, k and Fig. 9i with enlarged image). The translucent mineral also occurs in other parts of this sample, exhibiting different dimensions and apparently growing in concentric layers (Fig. 9j). The black mineral occurs not only associated with translucent mineral inclusions but also dispersed in the host diamond with an elongated disc shape (Fig. 9k).

Diamond JR5 presents a mineral inclusion with a subhedral habit and, according to SEM analysis, its composition contains Al, Fe, Ti, Si and O. Diamond JR7 has different compositions on its surface according to the backscattered SEM image, especially in areas with the presence of mineral inclusions. Near the edge of the crystal, a placoid mineral inclusion points to irregularities in the diamond habit, and SEM analysis identified the elements Fe, Ti, Al, Si and O in its composition. Diamond JR10 presents a mineral inclusion with a subhedral habit measuring 275 μm and the results of the semiquantitative spot chemical analysis performed on this mineral inclusion indicated the presence of Na, Si, Fe, K, Al, Mg, Mn, Ca, Ti and O.

6. Discussion

6.1. Diamond Records from the Serra do Espinhaço Province in the Earth´s Evolution

The morphology of diamonds carries a record of processes related to their history from formation to final positioning on the Earth's surface. This chapter presents evidence of endogenous processes (physiochemical environment in the mantle and metasomatism during the rise of the kimberlite) and exogenous processes (physical characteristics pertinent to surface transport) of diamonds from São João da Chapada and Jequitinhonha River.

The weathering and erosion of the kimberlite rock (after outcropping) makes residual minerals available for removal via transport. Residual minerals, depending on the local relief and regional base level, are transported in direct contact with the bedrock of the drainage substrate, which generates percussion marks and scratches resulting from abrasion during transportation (Tappert and Tappert, 2011). Abrasion marks are frequent and abundant on JR diamond surfaces (fig. 4g, h), given that the Jequitinhonha River has concentrated diamonds from the ruditic rocks of the SBf that outcrop along the central axis of the SER, carried after erosion by its tributaries on the left margin. The source rocks for the Jequitinhonha River diamonds therefore come from outcropping rocks from the diamond-bearing districts, which are between 30 and 65 km from the Areinha mine, the sampling site for diamonds from the JR set (Fig. 1).

On the other hand, the complete absence of abrasion textures in the São João da Chapada diamonds is indicative of an *in situ* or proximal primary source, although authentic kimberlite rocks are not yet known in the region. Nevertheless, Almeida-Abreu and Renger (2001), and Miranda et al. (2018) consider that the SBf quartzite metabreccias may represent the primary diamond rocks of the São João da Chapada-Campo Sampaio and Sopa-Guinda districts, therefore, considering them as vent breccias of phreatomagmatic eruptions, typical of intrusions that occur in water-saturated sedimentary successions. Reinforcing the proposition of a proximal or *in situ* source of SJ diamonds, the observations of Burnham et al. (2016) and Tappert et al. (2006), who reported placer deposits with low abundance of abraded diamonds (<15%) from primary kimberlite source areas located less than 50 km away.

As for the green coat on diamonds from SER´s diamondiferous districts (Fig. 3a, b and Fig. 4a, b, c, d), it seems related to prolonged exposure to radiation in the crustal environment (Chaves et al., 1996; Tappert and Tappert, 2011; Vance et al., 1973), originating from contact with radioactive groundwater from the host rock or from minerals rich in radioactive elements of the diamond deposit (Tappert and Tappert, 2011), while the brown spots seen in samples JR3 and JR4, may be due to the transformation of green spots after exposure to temperatures above 600 ºC (Vance et al., 1973).

However, these high temperatures cannot be attributed to regional metamorphism imposed on the rocks of the Espinhaço Supergroup, since the temperature of metamorphism in the central part of the SER, i. e, in the former coastal plain, did not exceed 450 ºC (Schöll and Fogaça, 1981). Therefore, exposure to a temperature of 600 ºC in the crustal environment would have been a specific process with a local effect. Green and brown radiation spots on diamond surfaces indicate recycling of buried secondary placers (paleo-collectors) (Burnham et al., 2016), and the presence of both spots together, seen in diamonds from the Jequitinhonha River (Fig. 4h), demonstrates that these diamonds were exposed to radiation at different times and therefore evidence their long and complex travel in the Earth's crust.

The fibrous texture observed in some SJ diamonds (Fig. 3) suggests rapid growth of highly carbon-saturated fluids in the mantle or within kimberlite magma (Tappert and Tappert, 2011) and these microscopic fibers may contain mineral inclusions (Fig. 3b, and Fig. 7e), the same situation described by Lang (1974). The fibrous layer in Fig. 7e shows a mineral phase that may be an aluminosilicate, but the fibrous layer of the diamond itself has a distinct composition according to the presence of Na, Mg, Al, and O. As most diamonds can react, to a certain extent point, with the kimberlite melt (Skvortsova et al., 2020), this mineral phase may have chemically interacted with this melt, not least because the chemical elements found in the layer contain abundant Mg, Ca and Si ions (Skvortsova et al., 2020). Aqueous KOH melt containing the mentioned ions can produce fine etching surface features, as seen in SJ2 diamonds (Fig. 6a) (Skvortsova et al., 2020), with the presence of minerals filling the etch feature ruts of SJ diamond surfaces being common (Fig. 4a,b, c) and given the frequency and abundance of quartz inside ruts (Fig. 7a, b, c, d, and Sd7), contact with Si-rich fluid in the environment crustal is demonstrated. However, as seen in Fig. 7e (sample SJ2), the etching features also cut minerals other than quartz and these etching channels are present in most diamonds from the SJ set which, in addition to distinguishing them from the JR set (Fig. 5), indicates that they underwent more effective dissolution (Fedortchouk, 2005).

Although fractures are common in diamonds from both SJ and JR sets, they have different origins, that is, while fractures in JR diamonds were formed during transport in a high-energy sedimentary environment (fluvial braided streams), the ruts on the SJ diamonds were originating from the fractures that have been widened by etching or resorption into kimberlite (Tappert and Tappert, 2011; Fedortchouk et al., 2005) in a subcrustal environment. Although the observation of a few hundred diamonds is recommended to identify the types of resorptions induced by kimberlite (Fedortchouk, 2019), in this study the recurrence of the features observed in most of the dozens of JR and SJ diamond samples presents itself as consistent evidence for the characterization of the types of reabsorption.

Ruts have also been frequently observed in diamond populations from Panda and Beartooth Kimberlites of Lac des Gras, Northwest Territories, Canada. A study carried out by Fedortchouk et al. (2005) correlated the development of these etch features of Panda and Beartooth diamonds with the crystallization temperature range and a high oxidation state (oxygen fugacity, here represented by log fO_2). For the volcanoclastic kimberlite Panda (which has a Serpentine-Dolomite matrix), the temperature varied from 1016 ºC to 1086 ºC, and log log fO_2 varied from -12.8 a -11.4, while for Beartooth, the temperature varied from 1018 ºC to 1036 ºC and log log fO_2 varied from -12.7 a - 12.4.

The values were calculated from Ol-Sp thermometry and oxybarometry (Ballhaus et al., 1991; Fedortchouk et al., 2005, 2009; Fedortchouk, 2019) and considering the physical similarities with the ruts of SJ diamonds, it can be assumed that the physicochemical conditions were similar to diamonds from Panda and Beartooth kimberlites. Furthermore, considering also other surface textures developed during kimberlite ascent, i.e., diamond´s preservation of its octahedral habit along with the development of etch features, such as deep pointed bottom truncated trigons as seen in sample JR3 and JR4 (Fig 4g and 6c), may correlate to low-pressure conditions and a high molar fraction carbon dioxide (XCO_2) among volatile fluids (Fedortchouk, 2019).

However, truncated trigons are not predominant in the JR set, where flat-bottomed negative trigons predominate (Fig. 4e, f) in both sets of diamonds, as can be seen in Supplemental Material Figures S6 and S7. The formation of predominantly shallow flat-bottomed trigons indicates the presence of H_20 dissolved in the fluids and/or melts (Fedortchouk, 2019), but temperature (T) can influence these trigon formation processes, as indicated by Fedortchouk (2015), who, using Atomic Force Microscopy, observed that trigons evolve from very regular profiles at low T to highly irregular profiles with multiple steps at higher T, and it was also observed that predominantly flat-bottomed trigons (f.b) evolve, in fluid with XCO_2 <~0.5, towards both f.b. and pointed bottomed trigons (with truncation), becoming common in all sizes at XCO_2 > ~0.5 CO_2, in the pressure range of 1–3 GPa (Fedortchouk, 2019).

In turn, it was observed in experimental studies carried out by Skvortsova et al. (2020) that aqueous solutions containing Sr, CO_2 + Ni/Co favor fewer formations of flat-bottomed triangles on a microscopic diamond surface, which therefore suggests that the trigons (which are mostly flat-bottomed) of diamonds SJ and JR studied were possibly originated in fluids rich in H_2O with XCO_2 < ~0.5 containing or not Sr, and CO_2 + Ni/Co.

Finally, the smooth surface textures, thin terraces and hillocks found in the same sample (JR3 - Fig. 6c, d), must have been formed under similar resorption conditions (Fedortchouk, 2019) and each of these features is related to diamond´s internal properties undergoing reabsorbing, since the hillocks derive from complexities of the internal structure, the pre-existing stepped faces are precursors of the

terraces, while the smooth surfaces develop on growth pattern (Tappert and Tappert, 2011; Fedortchouk, 2019). Therefore, it is assumed that the origin of the JR diamond hillocks and consequently the other features mentioned were the result of extensive resorption in a hydrous kimberlite melt at 1400 ºC (Skvortsova et al., 2020).

6.2. Nitrogen Aggregation and Model Temperatures

The studied diamonds of SJ and JR sets show relatively high nitrogen concentrations (ranging from 120 to 274 ppm) as well as relatively mature aggregation states (58% to 79% nitrogen as B aggregate). The reaction of these diamonds to ultraviolet light shows strong to very strong fluorescence, therefore compatible with nitrogen aggregation values (fluorescence images can be seen in Supplemental Figure S11). Remarkable is the high nitrogen content of diamonds from the SJ and JR sets when compared to that found in diamonds from Chapada Diamantina (Bahia, Brazil, supposedly of similar age to diamonds from the SER province), which ranged from undetectable to 172 ppm (Carvalho et al., 2018). On the other hand, the nitrogen values of SJ and JR diamonds are very similar to the concentrations and state of aggregation of diamonds from the South African Helam Mine (Kaapvaal Craton) described by McKenna et al. (2004), a common aggregation state in eclogitic and peridotite xenocrystal diamonds, which have been at mantle temperatures for billions of years (Shirey et al., 2013). The model temperature of the SJ and JR diamonds ranged from 1164 ºC to 1177 ºC, that is very similar to those determined for diamonds from the Helam Mine, are values consistent with long storage within the cratonic lithosphere (McKenna et al., 2004). Since these model temperatures do not consider the different diamond zones with different nitrogen concentrations and, in view that they can be affected by a short period of high temperature during the residence of diamonds in the mantle, it was therefore considered as an estimated value (Kohn et al., 2016). However, as all SJ and JR diamonds analyzed show “stepping” surface feature, it is possible to admit that at least the growth of these diamonds occurred slowly, under stable conditions in the mantle.

6.3. Mineral Inclusions: Hints of Mantle Source and Ascension Conditions

The first record of quartz as tabular intergrowths in a diamond from Brazil was made by Colony (1923), nevertheless, the curious occurrence of quartz in diamonds "as fracture-free" was described by Meyer and Svisero (1975). In most of the diamonds from the SJ set observe quartz inserted into the ruts described previously, like the mineral exposed on the surface of the SJ1 sample, which EDS analyses show homogeneous composition of silicon and oxygen (Fig. 7c, d), composition similar to those found in a cavity exposed in the polished section of sample SJ3 and in ruts of sample SJ2. Additionally, the Raman spectrum obtained for the quartz of the SJ1 diamond corresponds to the

alpha type spectrum (R040031) as per the RRuff database (additional data is provided in Supplemental data S12). It seems likely that the inclusion of quartz was caused by the destabilization of another mineral phase (coesite) during the rise of the kimberlitic magma, given that α-quartz is the phase with the lowest pressure and temperature of silica, therefore diverging from the environment of diamond crystallization. As already considered, syngenetic inclusions of quartz in diamonds are rare, given that the eventual availability of SiO_2 in the mantle environment crystallizes coesite and not quartz, however, inclusion of α-quartz in diamond has been reported (Yin et al., 2017 and references therein).

Two other hypotheses may clarify the presence of quartz in ruts and inside of SJ diamonds, since they appear to be very rutted: (i) a process of the thermal circulation of Si-rich fluids may have occurred after the formation of the corrosion features, related to regional metamorphism of the greenschist facies, associated or not with a hydrothermal event; (ii) at some point during the volcanic event, the circulation of hydrothermal solutions within the magma already in the crustal environment could have filled diamond ruts of the SJ set. Additionally, quartz inclusions were found in carbonado diamonds from Jequitinhonha River and isotopic results ($^{204}Pb/^{206}Pb$ vs. $^{207}Pb/^{206}Pb$) obtained by Chaves et al. (2005) suggest they were formed in a ~2.5-billion-year-old crustal environment.

Observations of the habit and color of opaque inclusions found in crystals JR10, JR3, JR5 and, JR7 (Fig. 9a to g), carried out with a petrographic microscope, indicated that they could be sulfides, biotite, oxides (Orlov, 1977; Titkov et al., 2003) or graphite, which is the most common inclusion in diamonds (Arima and Kozai, 2008; Khokhryakov et al., 2009). A chemical composition containing Al, Fe, Ti, Si and, O (seen on additional data on Supplemental data S9) is seen in the JR7 inclusion (Fig. 9c, e, f, g) and in the JR5 mineral inclusions (Fig. 9d) suggesting that this inclusion could be an almandine garnet, given that this mineral was once recognized in diamonds from Brazil (Meyer and Svisero, 1975). However, the orange color in the mentioned samples' inclusions (Fig. 9a, c, d) might indicate that they are pyrope garnets (Tappert and Tappert, 2011). An orange mineral is also seen in the fibrous coating of diamond SJ12, a mineral inclusion crystallized between its fibers (Lang, 1974). On this same layer a dark mineral inclusion is observed, which could be oxide, sulfide, or graphite according to its metallic luster. However, the characterization of the mentioned mineral phases and chemical formulas is still running.

The JR10 diamond contains a subhedral mineral inclusion whose chemical composition indicated by the SEM analysis is similar to that of clay minerals containing titanium, which suggests that it is a mineral phase that suffered destabilization as the magma rose or during its residence in the crustal environment, however, the precise definition of this mineral phase requires additional chemical analysis. On the other hand, qualitative chemical analyses indicate the presence of almandine garnet

and coesite and if quantitative chemical analyses confirm this indication, eclogitic paragenesis (cf. Tappert and Tappert, 2011; Shirey et al., 2013) for diamonds from the JR set will be proven.

Observations performed with a petrographic microscope allowed the identification of translucent mineral inclusions in the JR2 diamond (Fig. 9h, i, j) that were revealed as forsterites after FTIR spectrometric analyses (Fig. 8), consistent with their random orientation resulting from the previous existence of olivine before the introduction of the metasomatic fluid that crystallizes the diamond (Nestola et al., 2014; Milani et al., 2016; Nestola et al., 2017).

In turn, Bruno et al. (2016) observed that the low adhesion energies between diamond and forsterite close to invariance are due to the extremely low chemical affinity between these minerals and, therefore, no preferential orientation occurs during epitaxial growth in the diamond-forsterite system. In this same study, the protogenetic origin for olivine inclusions is proposed as the most plausible hypothesis, with the olivine-rich mantle rock of peridotite nature being percolated by carbon-rich fluid or melted to form diamonds. Nevertheless, the adhesion energies calculated by Bruno et al. (2016) did not consider a complex interface between diamond and forsterite, where a thin layer of fluid or 2D solid could occur. In our studies using optical microscopy, a layer was visualized between the forsterites and the face of the JR2 diamond that inserts them, which appears to be a mineral with the same composition as another mineral inclusion in this diamond (Fig. 9k), considering similar color and habit. The optical properties of this mineral inclusion suggest that it is a sulfide or graphite (Harris, 1972), but the lack of quantitative chemical data does not allow us to accurately confirm the mineral specimen.

Furthermore, Stachel and Harris (2008) based on the analysis of 5,000 lithospheric diamond inclusions, deduced that the geothermometry established by the aggregation of nitrogen and diamond inclusions indicates that the crystallization and mantle storage of peridotitic diamonds had occurred under the same thermal conditions, a similar situation, therefore, for JR diamonds, given their peridotite nature.

The geobarometry of peridotite inclusions refers to the crystallization temperature between 1150 and 1200 ºC (as also obtained for SJ and JR diamonds) and pressure of ~50 to 70 kbar (Stachel and Harris, 2008). However, this study also states that lithospheric diamonds from peridotitic sources crystallize under 65 kbar, corresponding to a depth of 200km in the Earth's crust, therefore, conditions that can be assumed for the crystallization of SJ and JR diamonds.

7. Conclusions

The diamonds studied in this work come from the Archean São Francisco Craton. The age of the SER diamonds is not known, although the emplacement of the kimberlite rocks of these diamonds is

estimated. In other words, SER diamond deposits in Precambrian (Statherian) rocks are restricted to rudites from the Sopa Brumadinho Formation (~1,700 Ma) with no known occurrence of diamonds in the region in rocks from stratigraphic units beneath or overlying the Sopa Brumadinho Formation. As the synsedimentary dikes of igneous rocks embedded in the Sopa Brumadinho Formation revealed U-Pb ages between 1680 and 1720 Ma, it is indicated that the diamond province of SER is the oldest on the planet.

The preliminary characterization of the mineral inclusions of SJ and JR diamonds demonstrates their lithospheric nature, which is consistent with their Paleoproterozoic emplacement age, given that all sublithospheric diamonds are of Mesoproterozoic or younger ages. The nature of the mineral inclusions observed in diamonds from the SJ e JR sets, as well as the frequent octahedral habit of the inclusions imposed by their diamond hosts (Fig. 3d, g, and 9a, e) typify their syngenetic origin within the peridotite lithospheric mantle. Thermobarometric studies of peridotite xenoliths and diamond mineral inclusions, as well as experimental studies of sampled diamonds originating from the base of the cratonic lithosphere, indicate temperatures of 1140–1170 °C and pressures of 5.0–6.1 GPa, parameters that can be considered for the crystallization environment of the studied SJ and JR diamonds.

Partial dissolution of SER diamond crystals is pervasive and must have occurred under the influence of volatiles. The flat-bottomed trigons in these diamonds indicate that, in the final stages of kimberlite emplacement H_2O-rich fluid with $XCO_2 < \sim 0.5$ reacted with the SJ and JR diamonds. The environment where the kimberlites of SJ diamonds were formed differs from that of JR diamonds, according to the common presence of ruts in the former. Some JR diamonds also show ruts, however, as they are diamonds from alluvial deposits, part of these diamonds (the green coated diamonds) come from rocks of the São João da Chapada district. Ruts may be related to highly oxidized kimberlites ($\log fO_2 \sim -12$), which had a crystallization temperature of approximately 1040 ºC.

Several of the SJ diamonds studied show α-quartz filling ruts and both ruts and α-quartz are encapsulated by the diamond, therefore the troughs and the quartz (SiO_2) must be considered syngenetic. The field stability of fayalite (Fe_2Si0_4) varies according to the chemical potentials of oxygen (μO_2), when low, the reaction is $Fe_2Si0_4 \leftrightarrow 2Fe + O_2 + Si0_2$ and when high (μO_2) by $3Fe_2Si0_4 + O_2 \leftrightarrow 3Fe_30_4 + 3Si0_2$ (O´Neill, 1987). As inclusions of opaque minerals are common (apparently, iron oxides predominate) in SER diamonds, it can be assumed that the α-quartz was produced by the reaction $Fe_2Si0_4 \leftrightarrow 2Fe + O_2 + Si0_2$, given that the α-quartz occupies the troughs of the ruts, which are the result of the partial dissolution of diamond crystals.

Since the Espinhaço orogenesis gave raise a tectonic stacking more than 8 km of rocks in the central part of the SER imposing regional metamorphism with temperatures of 450 ºC and pressures

of 4-5 Kb, it would therefore be possible that the chemical reaction $Fe_2Si0_4 \leftrightarrow 2Fe + O_2 + Si0_2$ occurred in the crustal environment due to regional metamorphism. The green coating of SJ diamonds is believed to have originated by the contact of radioactive groundwater with the host rock or by the presence of minerals rich in radioactive elements in the diamond deposit, which, in any case, reveals a long residence in the crustal environment. Another indication of retrograde metamorphism in SER diamond inclusions is the recurrent presence of clay minerals in ruts and microchannels, probably derived from metamorphic alteration of silicates (Fig. 4c, and 6a). Yin et al. (2017) recognized α-quartz inclusion in diamond of kimberlite from the North China Craton and suggested the possibility of inversion of the high-pressure polymorph, i.e., coesite, into α-quartz during rapid exhumation of the rocks.

The different textures and crystallographic features between SJ and JR diamonds (Fig. 5) demonstrate that, in fact, two distinct events of kimberlitic magmatism occurred. The first, to the west of the central area of SER, fed the intraformational conglomerates of the lower section of the Sopa Brumadinho Formation, which, according to its predominant well-rounded clasts, had its source area some tens of kilometers away from where the conglomerates outcrop. The second occurred *in situ*, as the breccias that occupy the top of the Sopa Brumadinho Formation appear as vent-breccias and, if not, their pelitic matrix and angular clasts report reworking diamond-bearing volcanic products located a few tens or hundreds of meters from where they are now exposed. SJ diamonds do not show abrasion or impact marks, reinforcing their autochthonous character, while all JR diamonds, transported by streams and rivers for more than 35 km from the exposure areas of the conglomerates and breccias of the Sopa Brumadinho Formation, have percussion marks and other typical abrasion features.

Acknowledgments

Master's student Anna C. Müller's scholarship was awarded by CAPES/UFVJM (project no. 88882.461706/2019-01). Funds from UFVJM and the CDTN covered the costs of the analyses, while other expenses were covered by Eduardo Fontana's and Pedro Angelo Almeida-Abreu's own funds. The authors express special thanks to the owners of Mineração Córrego Novo for providing the samples used in this study free of charge.

References

Almeida, F. F.; Hasui, Y.; Brito-Neves, .B.; Fuck, R. A., (1981). Brazilian structural provinces: an introduction. **Earth-Science Reviews**, 17, p. 1-19. https://doi.org/10.1016/0012-8252(81)90003-9**.**

Almeida-Abreu, P. A. (1993). A evolução geodinâmica da Serra do Espinhaço Meridional, Minas Gerais, Brasil [PhD. thesis]. University of Freiburg, 150 p. Freiburg.

Almeida-Abreu, P. A. (1996). O caminho das pedras: **Geonomos**, 4, p. 77-93.

Almeida-Abreu, P. A.; Renger, F. E. (2001). A origem dos diamantes da Serra do Espinhaço Meridional: o exemplo do distrito diamantífero de Sopa-Guinda (Diamantina-MG): **Revista Brasileira Geociências**, 31, p. 511-520, ISSN: 0375-7536.

Almeida-Abreu, P.A., and Renger, F. E. (2002). Serra do Espinhaço Meridional: um orógeno de colisão do Mesoproterozóico. **Revista Brasileira Geociências**, 32, p. 1-14. ISSN: 0375-7536

Almeida-Abreu, P. A.; Renger, F. E. (2007). Stratigraphy and facies of the southern Serra do Espinhaço, Minas Gerais, Brazil. **Zeitschrift der Deutschen Gesellschaft für Geowissenschaften**, 158, p. 9-29. https://doi.org/10.1127/1860-1804/2007/0158-0009.

Alvaro, M.; Angel, R. J.; Nestola, F. (2022). Inclusions in diamonds probe Earth's chemistry through deep time. **Communications Chemistry**, 5, p. 1-3, https://doi.org/10.1038/s42004-022-00627-1.

Amaral-Santos, E.; Jelinek, A. R.; Almeida-Abreu, P. A. (2022). Denudation rates of the southern Espinhaço range basement, southeastern Brazil, constrained by apatite fission-track thermochronology: South American Symposium on Isotope Geology, 12th, Abstracts, p. 97. Santiago, Chile.

Arima, M., and Kozai, Y. (2008). Diamond dissolution rates in kimberlitic melts at 1300–1500 ºC in the graphite stability field. European Journal Mineralogy, 20, p. 357-364. https://doi.org/10.1127/0935-1221/2008 /0020-1820.

Babu, E. V. S. S. K.; Dash, S.; Santhosh, G. H. N. V.; Mukherjee, A. (2023). Origin of clinopyroxene megacrysts from the 1.1 Ga Chigicherla-4 kimberlite (CC4), Dharwar craton, southern India: Implications for multi-stage metasomatism of the sub-continental lithospheric mantle: **Journal Asian Earth Science**, 244. https://doi.org/10.1016/j.jseaes. 2022.105534.

Benitez, L. (2009). Províncias diamantíferas de Minas Gerais: uma proposta para a caracterização de populações de diamantes típicas como subsídio à Certificação Kimberley [PhD. Thesis]. Universidade Federal de Minas Gerais, 223 p. Belo Horizonte.

Bezerra-Neto, F. E. (2016). Estudo de rochas exóticas da Formação Sopa-Brumadinho e possíveis implicações para a fonte dos diamantes do Espinhaço Meridional [Master´s dissertation]. Universidade de Brasília, 105 p. Brasília.

Boyd, S. R.; Kiflawi, I.; Woods, G. S. (1994). The relationship between infrared absorption and the A defect concentration in diamond: Philosophical Magazine, 69, p. 1149-1153. https://doi.org/10.1080/01418639408240185

Boyd, S. R.; Kiflawi, I.; Woods, G. S. (1995). Infrared absorption by the B nitrogen aggregate in diamond. **Philosophical Magazine**, 72, p. 351-361. https://doi.org/10.1080/13642819508239089.

Bruno, M.; Rubbo, M.; Aquilano, D.; Massaro, F. R.; Nestola, F. (2016). Diamond and its olivine inclusions: a strange relation revealed by ab initio simulations: **Earth Planetary Science Letters**, 435, p. 31-35. https://doi.org/10.1016/j.epsl. 2015.12.011.

Burnham, A. D.; Bulanova, G. P.; Smith, C. B.; Whitehead, S. C.; Kohn, S. C.; Gobbo, L.; Walter, M. J. (2016). Diamonds from the Machado River alluvial deposit, Rondônia, Brazil, derived from both lithospheric and sublithospheric mantle. **Lithos**, 265, p. 199-213, https://doi.org/10.1016/j.lithos.2016.05.022**.**

Carvalho, L. D. V. D.; Schnellrath, J.; Medeiros, S. R. D. (2018). Mineral inclusions in diamonds from Chapada Diamantina, Bahia, Brazil: a Raman spectroscopic characterization. **Revista Escola de Minas - UFOP**, 71, p. 27-35. https://doi.org/10.1590/0370-44672016710160.

Chaves, M. L. S. C.; Svisero, D. P. (1993). Características geológicas e origem dos conglomerados diamantíferos das regiões de Diamantina (Mesoproterozóico) e de Romaria (Cretáceo Superior), **Boletim Geosciências, USP, Série Científica**, 24, p. 49-57. Minas Gerais. https://doi.org/10.11606/issn.2316-8986.v24i0p49-57.

Chaves, M. L. S. C.; Geraldes, M. C.; Sano, Y.; Chambel, L. (2005). Primeiros resultados da datação Pb-Pb em diamantes carbonados da Chapada Diamantina (BA) e Rio Jequitinhonha (MG), Serra do Espinhaço. **Revista Brasileira Geociências**, 35, p. 419-422, ISSN: 0375-7536.

Chaves, M. L. S. C.; Karfunkel, J.; Svisero, D. P. (1998). Sobre a polêmica da origem do diamante na Serra do Espinhaço (Minas Gerais): um enfoque mineralógico. **Revista Brasileira Geociências**, 28, p. 285-294, ISSN: 0375-7536

Chaves, M. L. S. C.; Karfunkel, J.; Banko, A.; Stasiulevicius, R.; Svisero, D. P. (1996). Diamantes de capa verde: freqüência, distribuição e possível origem nos depósitos diamantíferos de Minas Gerais: **Boletim Instituto Geociências, USP, Série Científica**, 27, p. 51-60. https://doi.org/10.11606/issn.2316-8986.v27i0p51-60

Colony, R. J. (1923). The final consolidation phenomena in the crystallization of igneous rock: **Journal of Geology**, 31, p. 169-178.

Correns, W. C. (1932). Über die Diamantlagerstãtten des Hochlandes von Diamantina, Minas Gerais, Brasilien: **Zeitschrift für Praktische Geologie**, 40, p.161-168, 177-192.

Dossin, I. A.; Dossin, T. M.; Charvet, J.; Cocherie, A.; Rossi, P. (1993). Single-Zircon dating by stepwise Pb-evaporation of Middle Proterozoic magmatism in the Espinhaço Range, southeastern São Francisco Craton (Minas Gerais, Brazil): Simpósio sobre o Cráton do São Francisco, 2th, Salvador, **Anais**, p. 39-42.

Dossin, I.A.; Uhlein, A.; Dossin, T. M., (1984). Geologia da faixa móvel Espinhaço em sua porção Meridional – MG: Congresso Brasileiro de Geologia, 33th, Rio de Janeiro, **Anais**, 2, p. 3118–3132.

Fedortchouk, Y. (2015). Diamond resorption features as a new method for examining conditions of kimberlite emplacement: **Contributions to Mineralogy and Petrology**, 170, p. 36, https://doi.org/10.1007/s00410-015-1190-z

Fedortchouk, Y. (2019). A new approach to understanding diamond surface features based on a review of experimental and natural diamond studies: **Earth-Science Reviews**, 193, p. 45-65, https://doi.org/10.1016/j.earscirev.2019.02.013

Fedortchouk, Y.; Canil, D. (2009). Diamond oxidation at atmospheric pressure: development of surface features and the effect of oxygen fugacity: **European Journal of Mineralogy**, 21, p. 623-635, https://doi.org/10.1127/0935-1221/2009/0021-1929

Fedortchouk, Y.; Canil, D.; Carlson, J. A. (2005). Dissolution forms in Lac de Gras diamonds and their relationship to the temperature and redox state of kimberlite magma. **Contributions to Mineralogy and Petrology**, 150, p. 54-69. https://doi.org/10.1007/s00410-005-0003-1.

Gernon, T. M.; Jones, S. M.; Brune, S. et al. (2023). Rift-induced disruption of cratonic keels drives kimberlite volcanism. **Nature**. https://doi.org/10.1038/s41586-023-06193-3.

Hagedorn, M. G. (2004). Contexto Geotectônico da Serra do Espinhaço e domínios adjacentes a leste (Minas Gerais) com ênfase em aspectos geoquímicos e geocronológicos [PhD. thesis]. Universidade Estaual Paulista, 222 p. Rio Claro, São Paulo.

Harris, J. W. (1972). Black material on mineral inclusions and in internal fracture planes in diamond. **Contributions to Mineralogy and Petrology**, 35, p. 22-33, https://doi.org/10.1007/BF00397374.

Herrgesell, G.; Pflug, R. (1986). The Thrust Belt of the Southern Serra do Espinhaço, Minas Gerais, Brazil. **Zentralblatt für Geologie und Paläontologie**, 9-10, p. 1405-1414. https://doi.org/10.1127/zbl_geol_pal_1/1985/1986/1405.

Howell, D.; Griffin, W. L.; Piazolo, S. et al. (2013). A spectroscopic and carbon-isotope study of mixed-habit diamonds: Impurity characteristics and growth environment. **American Mineralogist**, 98, p. 66-77. https://doi.org/10.2138/am.2013.4179.

Khokhryakov, A. F.; Nechaev, D. V.; Sokol, A. G.; Palyanov, Y. N. (2009). Formation of various types of graphite inclusions in diamond: Experimental data: **Lithos**, 112, p. 683-689. https://doi.org/10.1016/j.lithos.2009.05.010.

Knauer, L. G. (1990). Evolução geológica do Precambriano da porção centro leste da Serra do Espinhaço Meridional e metalogênese associada Dissertação de mestrado. Universidade de Campinas, São Paulo, 115 p. Campinas.

Kohn, S. C.; Speich, L.; Smith, C. B.; Bulanova, G. P. (2016). FTIR thermochronometry of natural diamonds: A closer look: Lithos, v. 265, p. 148-158. https://doi.org/10.1016/j.lithos.2016.09.021.

Lafuente, B.; Downs, R. T.; Yang, H.; Stone, N. (2015). The Rruff Project: power databases RRUFF Proj. Armbruster, T., and Danisi, R.M. (eds), Highlights Mineralogy and Crystallography, ISBN 978-3-11-041711-1.

Lang, A. R. (1974). Glimpses into the growth history of natural diamonds. **Journal of Crystal Growth**, 24, 25, p. 108-115. https://doi.org/10.1016/0022-0248(74)90287-5.

Lefebvre, N.; Kopylova, M.; Kivi, K. (2005). Archean calc-alkaline lamprophyres of Wawa, Ontario, Canada: unconventional diamondiferous volcaniclastic rocks: **Precambrian Research**, 138, p. 57-87. https://doi.org/10.1016/j. precamres.2005.04.005.

Martins-Neto, M. A. (1998). O Supergrupo Espinhaço em Minas Gerais: registro de uma bacia rifte-sag do Paleo/Mesoproterozóico. **Revista Brasileira Geociências**, 48, p. 151-168, ISSN: 0375-7536.

Martins-Neto, M. A. (2009). Sequence stratigraphic framework of Proterozoic successions in eastern Brazil. **Marine and Petroleum Geology**, 26, p. 163-176. https://doi.org/10.1016/j.marpetgeo.2007.10.001.

McKenna, N.; Gurney, J. J.; Klump; Davidson, J. M. (2004). Aspects of diamond mineralization and distribution at the Helam Mine, South Africa: **Lithos**, 77, p. 193-208, https://doi.org/10.1016/j.lithos.2004.04.004.

Meyer, H. O.; Svisero, D. P. (1975). Mineral inclusions in Brazilian diamonds, *in* Physics and Chemistry of the Earth, Pergamon Press, p. 785-795. Oxford, UK.

Milani, S.; Nestola, F.; Angel, R. J.; Nimis, P.; Harris, J. W. (2016). Crystallographic orientations of olivine inclusions in diamonds: **Lithos**, 265, p. 312-316, https://doi.org/10.1016/j.lithos.2016.06.010.

Miranda, R. F. (2019). Caracterização geológica das metabrechas quartzíticas da Formação Sopa Brumadinho- MG: Um estudo de caso das lavras Brumadinho e Córrego Novo. Dissertação de mestrado. Universidade Federal dos Vales do Jequitinhonha e Mucuri, 77 p. Diamantina.

Miranda**,** R**.** F**.;** Battilani, G. A.; Almeida-Abreu, P. A. (2018)**.** Geologia das metabrechas diamantíferas na Formação Sopa-Brumadinho, Serra do Espinhaço Meridional, MG: 7th Simpósio Brasileiro de Geologia do Diamante, 7th, **Anais**, p. 1-4. Salvador, Bahia.

Nestola, F.; Jung H.; Taylor, L. A. (2017). Mineral inclusions in diamonds may be synchronous but not syngenetic: **Nature Communications**, 8, p. 1-6. https://doi.org/10.1038/ncomms14168.

Nestola, F.; Nimis, P.; Angel, R. J.; Milani, S.; Bruno, M.; Prencipe, M.; Harris, J. W. (2014). Olivine with diamond-imposed morphology included in diamonds. Syngenesis or protogenesis?: **International Geology Review**, 56, p. 1658-1667, https://doi.org/10.1080/00206814.2014.956153.

O´Neil, H. St. C. (1987). Quartz-fayalite-iron and quartz-fayalite-magnetite equilibria and the free energy of formation of fayalite (Fe_2Si0_4) and magnetite (Fe_30_4): **American Mineralogist**, 72, p. 67-75.

Orlov, I. L. (1977). The mineralogy of the diamond: John Wiley & Sons Inc, New Jersey, 235 p., ISBN:0471018694, 9780471018698.

Pflug, R. (1968). Observações sobre a estratigrafia da Série Minas na região de Diamantina, Minas Gerais: Boletim da Divisão de Geologia e Mineralogia, Departamento Nacional da Produção Mineral, Rio de Janeiro, **Nota Preliminar de Estudos**, 142, p. 1-20.

Pintér, Z.; Foley, S. F.;Yaxley, G. M. (2022). Diamonds, dunites, and metasomatic rocks formed by melt/rock reaction in craton roots. **Ccommunications Earth & Environment**, 3(296), https://doi.org/10.1038/s43247-022-00630-3.

Projeto Espinhaço (1997) Geologia da Folha Diamantina (by A. C. C. Fogaça), *in*, Grossi-Sad, J.H. et. al (eds), Arquivos em CD-ROM (textos, mapas e anexos), Companhia. Mineradora de Minas Gerais, Belo Horizonte.

Renger, F. E. (2005). Regimes de extração e produção de diamantes do Serro Frio no século XVIII: Simpósio Brasileiro Geologia do Diamante, 4th, *in* Almeida-Abreu, P.A., Abreu, F.R., (eds), Sociedade Brasileira de Geologia, Núcleo de Minas Gerais, **Boletim**, 14, p. 139-142.

Rolim, V. K.; Rosière, C. A.; Santos, J. O. S.; McNaughton, N. J. (2016). The Orosirian-Statherian banded iron formation-bearing sequences of the southern border of the Espinhaço Range, Southeast Brazil: **Journal of South American Earth Science**, 65, p. 43-66. https://doi.org/10.1016/j.jsames.2015.11.003.

Schöll, W. U.; Fogaça, A. C. C. (1979). Estratigrafia da Serra do Espinhaço na região de Diamantina: Simpósio de Geologia de Minas Gerais, 1th, Diamantina, Minas Gerais, **Anais**, p. 276-290.

Schöll, W. U.; Fogaça, A. C. C. (1981). Geologia das Quadrículas Guinda e Gouveia, scale 1:25,000. Departamento Nacional de Produção Mineral (DNPM – Ministério das Minas e Energia), Projeto Mapeamento do Espinhaço Meridional, Diamantina e Belo Horizonte, Minas Gerais/MG, 63 p.

Shirey, S. B.; Cartigny, P.; Frost, D. J. et al. (2013). Diamonds and the geology of mantle carbon. **Reviews in Mineralogy and Geochemistry**, 75, p. 355-421, https://doi.org/10.2138/rmg.2013.75.12

Skvortsova, V. L.; Shiryaev, A. A.; Fedortchouk, Y. (2020). Influence of ions on diamond resorption. **Diamond and Related Materials**, 104, 107764, https://doi.org/10.1016/j.diamond.2020.107764.

Smart, K. A.; Tappe, S.; Stern, R. A.; Webb, S. J.; Ashwal, L. D. (2016). Early Archaean tectonics and mantle redox recorded in Witwatersrand diamonds: **Nature Geoscience**, 9, p. 255-259. https://doi.org/10.1038/NGEO2628

Smit, K. V.; Timmerman, S.; Aulbach, S.; Shirey, S. B.; Richardson, S. H.; Phillips, D.; Pearson, D. G. (2022). Geochronology of Diamonds: **Reviews in Mineralogy and Geochemistry**, 88, p. 567-636, https://doi.org/10.2138/rmg.2022.88.11.

Speich, L.; Kohn, S. C. (2020). QUIDDIT-Quantification of infrared active defects in diamond and inferred temperatures: **Computers & Geosciences**, 144, 104558, https://doi.org/10.1016/j.cageo. 2020.104558.

Speich, L.; Kohn, S. C.; Bulanova, G. P.; Smith, C. B. (2018). The behaviour of platelets in natural diamonds and the development of a new mantle thermometer. **Contributions Mineralogy and Petrology**, 173, p. 1-21, https://doi.org/10.1007/s00410-018-1463-4.

Stachel, T.; Harris, J. W. (2008). The origin of cratonic diamonds — Constraints from mineral inclusions. **Ore Geology Reviews**, 34, p. 5-32. https://doi.org/10.1016/ j.oregeorev.2007.05.002.

Svisero, D. P. (2006). As múltiplas facetas do diamante: **Revista USP**, 71, p. 52-69, https://doi.org/ 10.11606/issn.2316-9036.v0i71p52-69.

Tappert, R.; Tappert, M. C. (2011). Diamonds in nature: a guide to rough diamonds: **Springer Science & Business Media**, 140 p. Berlin. https://doi.org/10.1007/978-3-642-12572-0.

Tappert, R.; Stachel, T.; Harris, J. W.; Muehlenbachs, K.; Brey, G. P. (2006). Placer diamonds from Brazil: indicators of the composition of the earth's mantle and the distance to their kimberlitic sources: **Economic Geology**, 101, p. 453-470. https://doi.org/10.2113/ gsecongeo.101.2.453.

Taylor, W.R., Canil, D., and Milledge, H.J., 1996, Kinetics of Ib to IaA nitrogen aggregation in diamond: Geochimica et Cosmochimica Acta, v. 60, p. 4725-4733, https://doi.org/10.1016/ S0016-7037(96)00302-X.

Taylor, W. R.; Jaques, A. L.; Ridd, M. (1990). Nitrogen-defect aggregation characteristics of some Australasian diamonds; time-temperature constraints on the source regions of pipe and alluvial diamonds. **American Mineralogist**, 75, p. 1290-1310, https://doi.org/0003-004X/90/1112-1290$02.00.

Timmerman, S.; Reimink, J. R.; Vezinet, A. et al. (2022). Mesoarchean diamonds formed in thickened lithosphere, caused by slab-stacking. **Earth Planetary Science Letters**, v. 592, https://doi.org/ 10.1016/j.epsl.2022.117633.

Titkov, S. V.; Zudin, N. G., Gorshkov, A.I.; Sivtsov, A.V.; Magazina, L. O. (2003). An investigation into the cause of color in natural black diamonds from Siberia. **Gems & Gemology**, 39, p. 200-209, https://doi.org/10.5741/GEMS.39.3.200.

Uhlein, A.; Trompette, R.; Egydio-Silva, M. (1998). Proterozoic rifting and closure, SE border of the São Francisco Craton, Brazil. **Journal of African Earth Science**, 11, p. 191-203. https://doi.org/10.1016/S0895-9811(98)00010-8.

Vance, E. R.; Harris, J. W.; Milledge, H. J. (1973). Possible origins of α-damage in diamonds from kimberlite and alluvial sources. **Mineralogical Magazine**, 39, p. 349-360. https://doi.org/10.1017/minmag.1973.039.303.12.

Walter, M. J.; Thomson, A. R.; Smith, E. M. (2022). Geochemistry of Silicate and Oxide Inclusions in Sublithospheric Diamonds. **Reviews in Mineralogy & Geochemistry**, 88, p. 393-450. http://dx.doi.org/10.2138/rmg.2022.88.07.

Yin, Z.; Jiang, C.; Chen, M.; Lu, F.; Chen, Q. (2017). Inclusions of α-quartz, albite and olivine in a mantle diamond. **Gondwana Research**, 44, p. 228-235. https://doi.org/10.1016/j.gr.2016.12.004.

Supplemental Material

Table of Content:

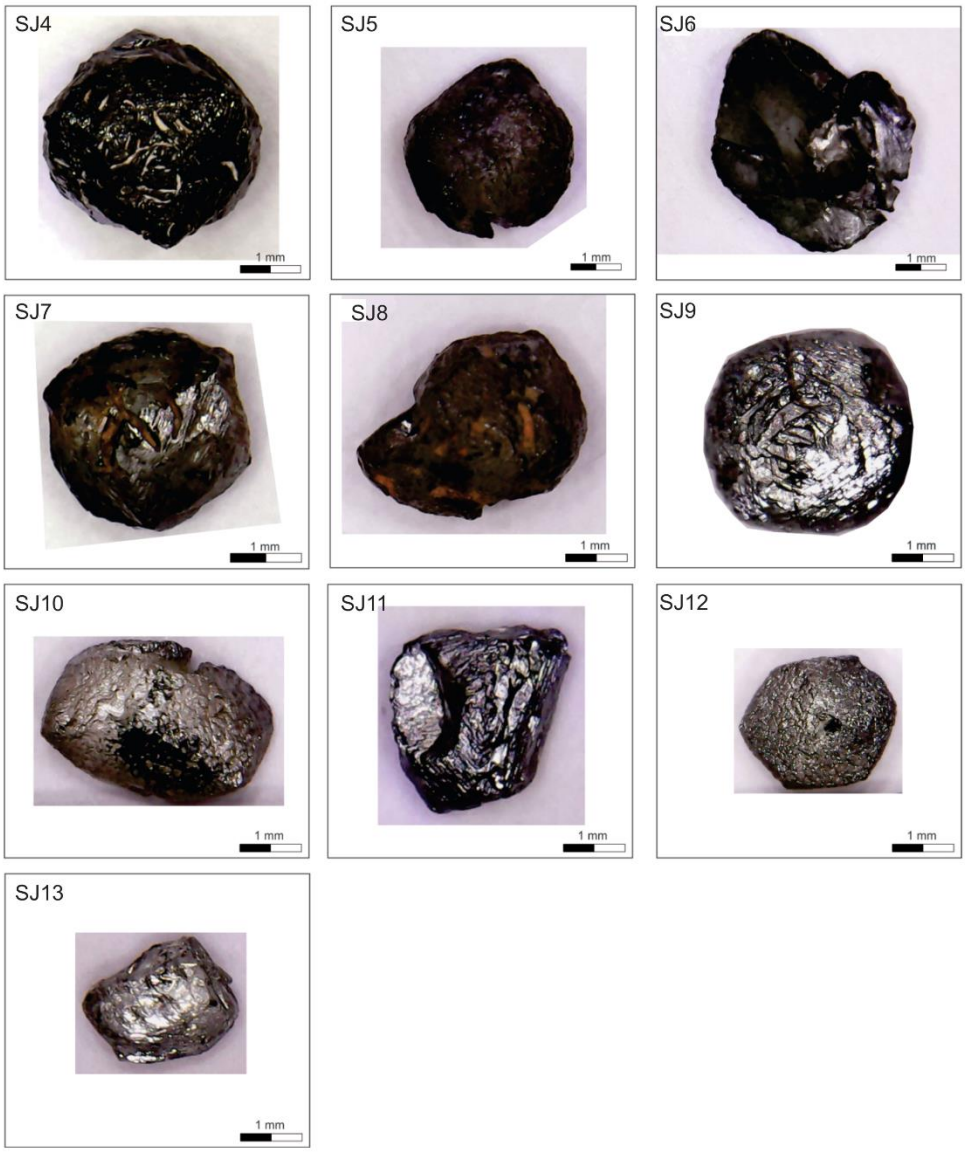

Figure S1. Photographs of the SJ diamond's set in their original form. The presence of surfaces with green coating or green spots on SJ diamonds is frequent.

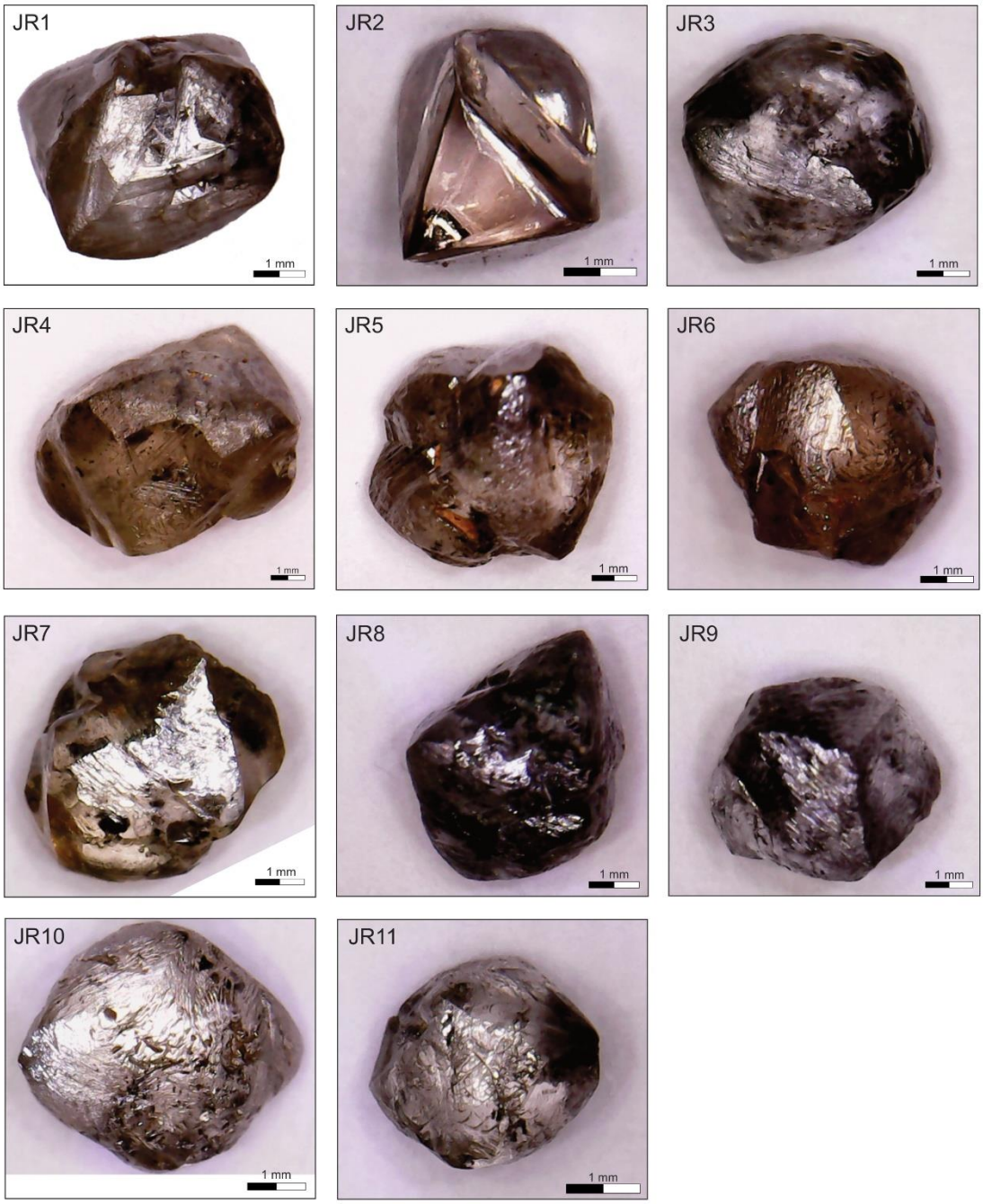

Figure S2. Photographs of the JR diamond's set in their original form. The frequent presence of impact marks on the surfaces of the diamonds can be observed.

Figure S3. Above: main pit of the Córrego Novo Mining operation in October 2023. Below: detail of the diamond bearing quartzite breccia with its pelitic matrix.

Figure S4. Google Earth image showing the location of Córrego Novo Mining, the sampling site for SJ diamonds.

Figure S5. Google Earth image showing the location of the Areinha mines on the Jequitinhonha River, the sampling site for SR diamonds.

	SJ4	SJ5	SJ6	SJ7	SJ8	SJ9	SJ10	SJ11	SJ12	SJ13
Trigons	X	X		X	X	X				X
Stepping	X			X	X	X		X		X
Frost		X		X			X	X	X	X
Ruts	X	X	X	X	X	X	X	X		
Twinning	X			X	X	X				
Green spots	X		X	X						
Green coating	X			X	X	X		X	X	X
Minerals in cavities	X	X	X	X	X	X	X	X	X	X
Fractures	X	X	X	X	X	X		X		

Figure S6. Table listing features and characteristics found in SJ diamonds, obtained from the Córrego Novo Mining pits.

	JR1	JR2	JR3	JR4	JR5	JR6	JR8	JR8	JR9	JR10	JR11
Trigons	X	X	X	X	X	X	X	X		X	X
Stepping	X	X	X	X	X	X	X	X	X	X	X
Hillocks			X								
Frost	X		X	X	X	X	X		X	X	
Percussion marks	X		X	X	X	X			X	X	X
Scratch marks			X				X			X	X
Edge abrasion						X					
Green spots		X	X	X				X	X		
Brown spots			X	X							
Green coating			X		X	X		X		X	
Minerals in cavities			X	X		X		X	X		X
Fractures		X	X		X	X		X			

Figure S7. Table listing features and characteristics of JR diamonds from Areinha mine pits.

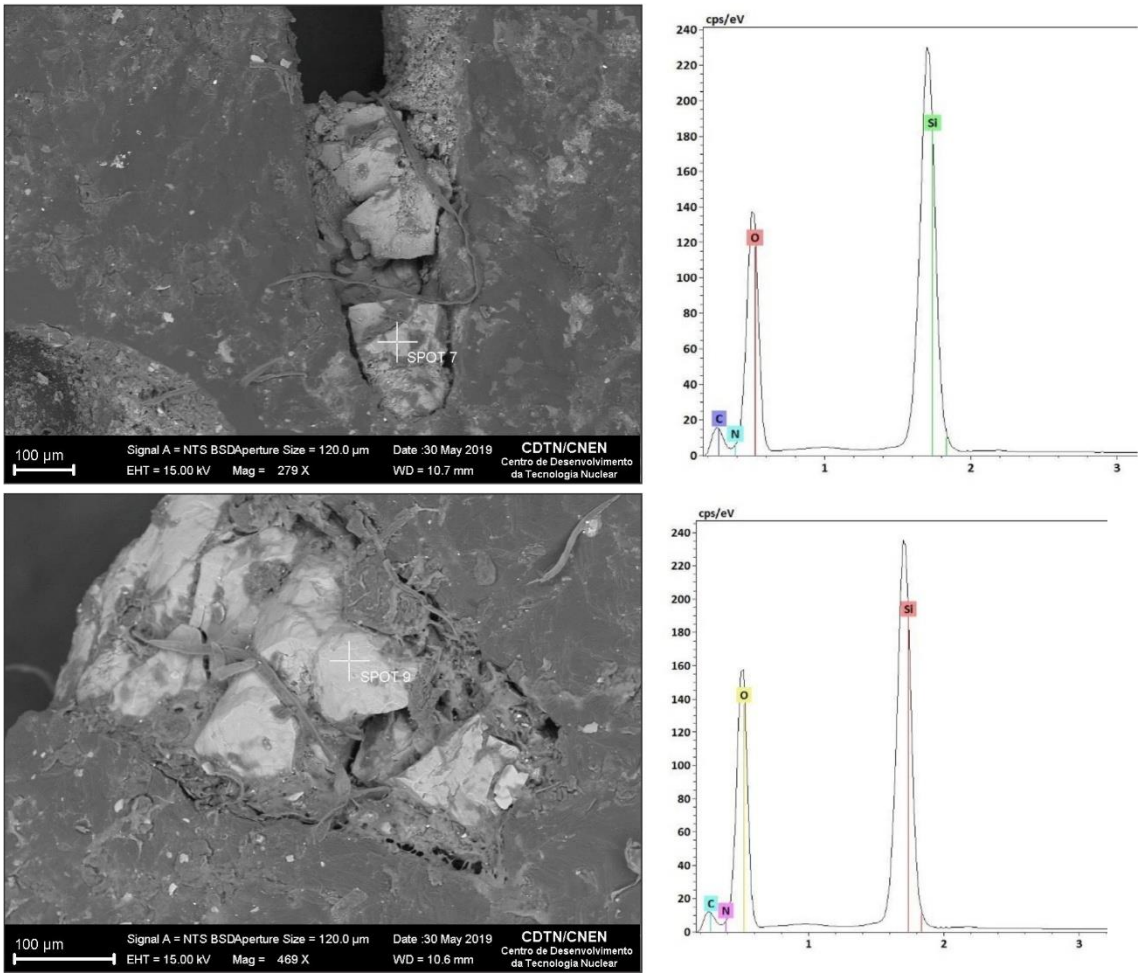

Figure S8. Scanning Electron Microscope (SEM) images showing quartz filling a rut in an SJ1 diamond. On the right, SEM spectral graphs with Si and O peaks, revealing that it is quartz.

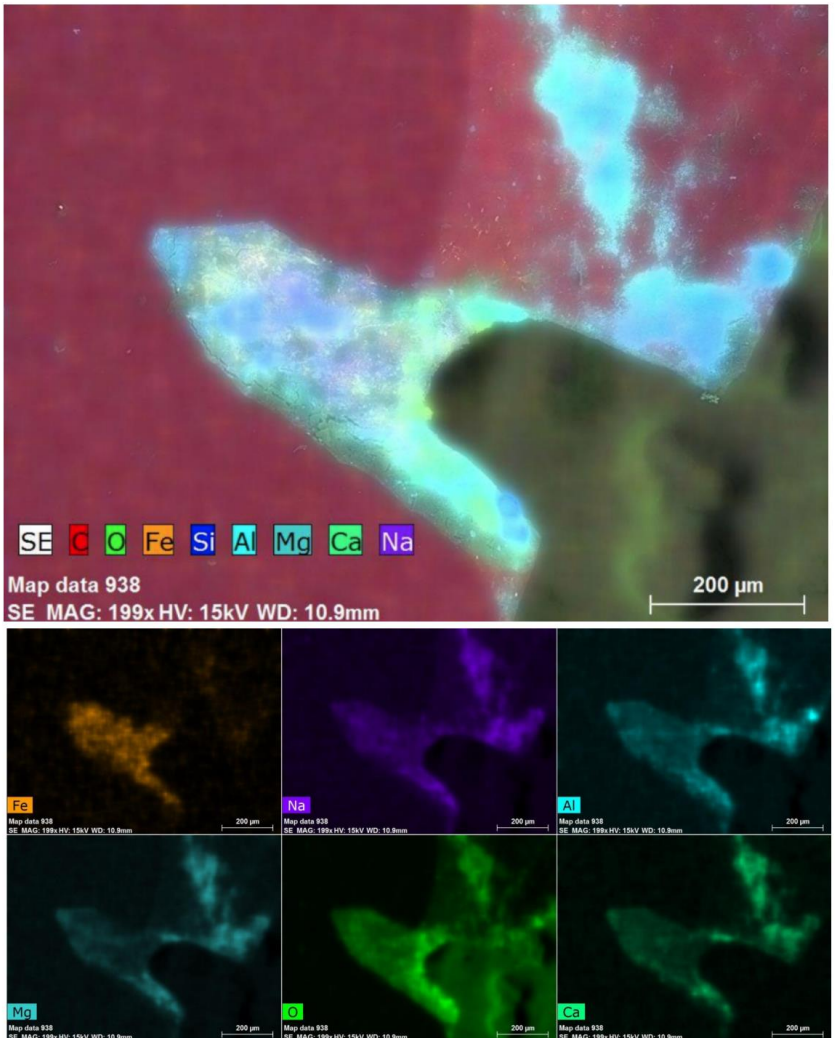

Figure S9. Top panel figure: SEM image of a dipyramidal mineral embedded in a layer of diamond SJ2 showing the map of the chemical elements (C, O, Fe, Si, Al, Mg, Ca, Na). The other images in the panel show individual maps of the chemical elements O, Na, Mg, Fe, Ca, and Al, respectively.

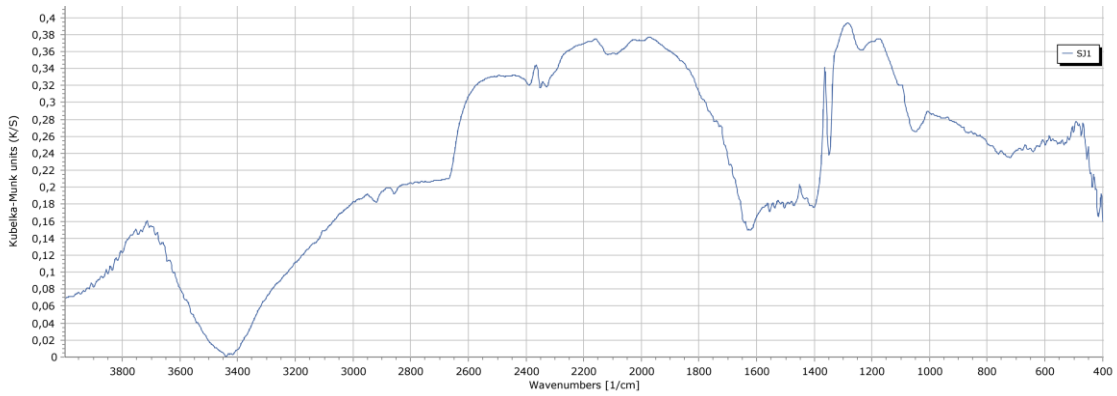
SJ1
Kubelka-Munk units (K/S)
Wavenumbers [1/cm]

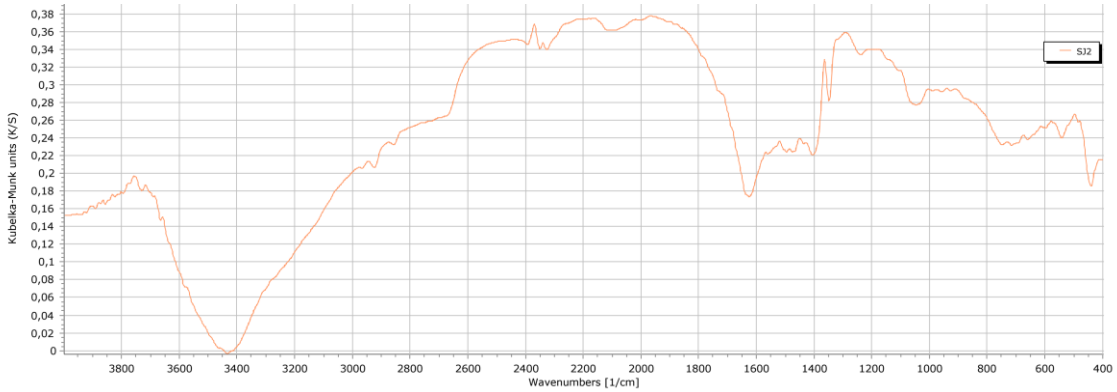
SJ2
Kubelka-Munk units (K/S)
Wavenumbers [1/cm]

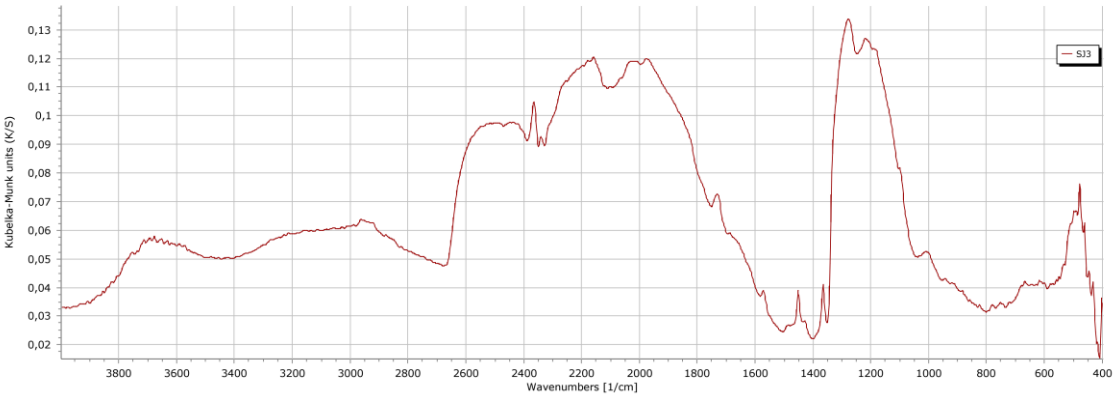
SJ3
Kubelka-Munk units (K/S)
Wavenumbers [1/cm]

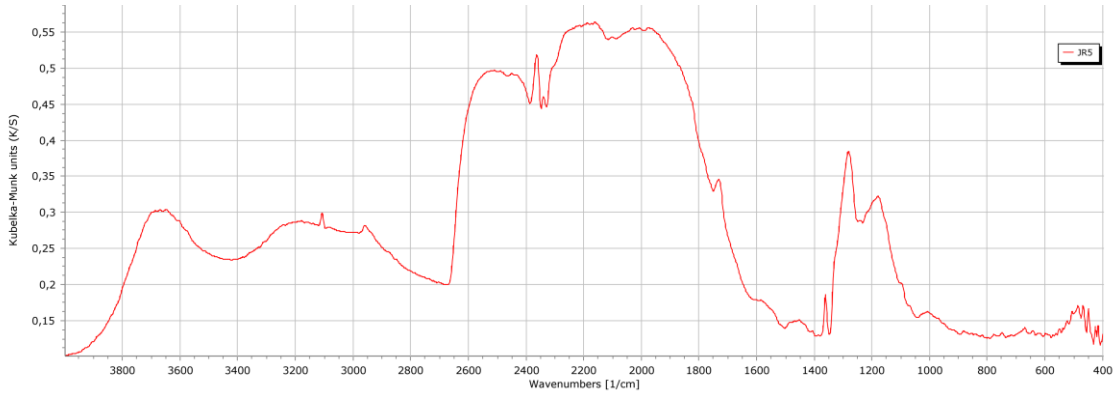
JR5
Kubelka-Munk units (K/S)
Wavenumbers [1/cm]

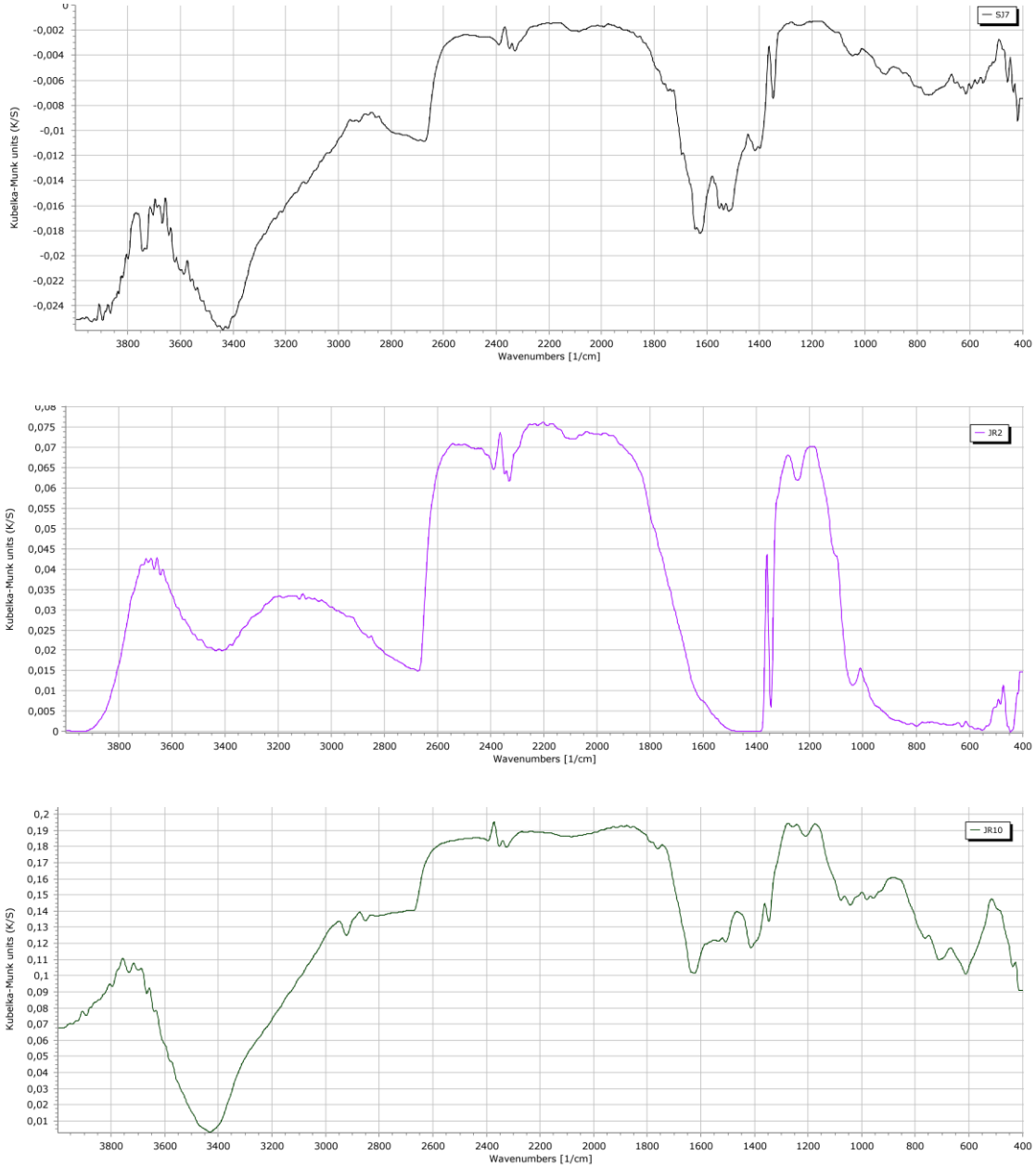

Figure S10. Fourier-transform infrared (FTIR) spectra of diamonds from the Jequitinhonha River (JR) and São João da Chapada district (SJ). Absorbance values are presented in Kubelka–Munk units (K/S) as a function of wavenumber (cm^{-1}). Each plot corresponds to a distinct diamond grain. The spectra highlight variations in structural defects among samples from different sources in the Serra do Espinhaço region.

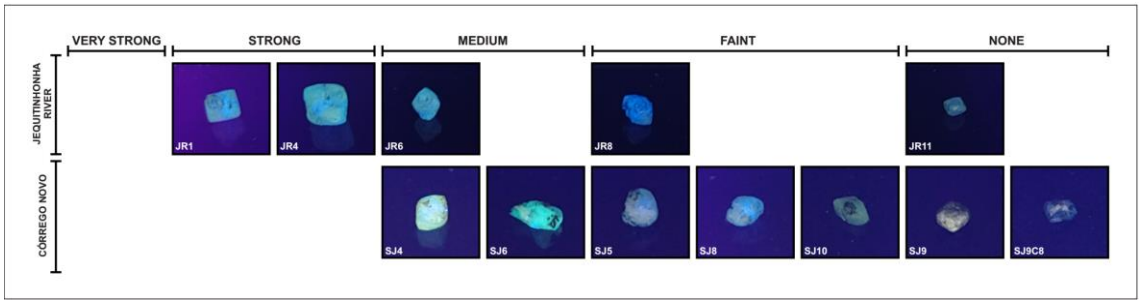

Figure S11. Ultraviolet light fluorescence of JR and SJ diamonds, arranged in decreasing order of fluorescence intensity.

Raman Conditions	
	Wavelength
Quartz (RRUFF R040031)	532 nm
Mineral inside ruts	532 nm

Figure S12. Graph of the Raman spectrum obtained from the mineral included in the SJ1 diamond (in red) and the spectrum of alpha quartz (R040031) from the RRuff database (in blue).